View metadata, citation and similar papers at core.ac.uk

brought to you by CORE

provided by VCU Scholars Compass

Virginia Commonwealth University

VCU Scholars Compass

Theses and Dissertations

Graduate School

2014

Developing a Caenorhabditis elegans Model for Marfan Syndrome

Pauline Fotopoulos

Virginia Commonwealth University

Follow this and additional works at: https://scholarscompass.vcu.edu/etd

 Part of the Biochemistry, Biophysics, and Structural Biology Commons

© The Author

Downloaded from

https://scholarscompass.vcu.edu/etd/631

This Thesis is brought to you for free and open access by the Graduate School at VCU Scholars Compass. It has been accepted for inclusion in Theses and Dissertations by an authorized administrator of VCU Scholars Compass. For more information, please contact libcompass@vcu.edu.

© Pauline Effie Andreas Fotopoulos May, 2014

All Rights Reserved

Developing a *Caenorhabditis elegans* Model for Marfan Syndrome

A thesis submitted in partial fulfillment of the requirements for the degree of Master of Science in Biochemistry and Molecular Biology at Virginia Commonwealth University.

by

Pauline Effie Andreas Fotopoulos
Bachelor of Science in Biology
James Madison University 2008-2012

Director: Young-Jai You Ph.D.

Department of Biochemistry and Molecular Biology

Virginia Commonwealth University
Richmond, Virginia
April, 2014

Acknowledgement

I wish to thank my advisor Dr. Young You who discovered the *mua-3* phenotype, and is both an exceptional scientist and mentor. Jeong Ho Kim determined the temperature sensitivity of the *mua-3* phenotype and performed mapping. I would like to thank and acknowledge my committee members Dr. Leon Avery, Dr. Jessica Bell, and Dr. Young You. I would also like to thank my lab members, Dr. Thomas Gallagher, Jheesoo Ahn, Kristen Davis, Divya Padmanbha, and Inwhan Lee. Additionally I wish to thank Commander Demetri Economos Ph.D.

TABLE OF CONTENTS

List of Tables

List of Figures

List of Abbreviations

1. TGF-β - Transforming Growth Factor Beta

2. BMP- Bone Morphogenic Protein

3. cGMP- cyclic guanosine monophosphate

4. PKG- cGMP Dependent Protein Kinase

5. MFS- Marfan Syndrome

6. ECM- Extracellular Matrix

7. WAT- White Adipose Tissue

8. BAT- Brown Adipose Tissue

9. BA- Beige Adipocytes

10. HMM- Hidden Markov Model

11. SODD- Suppressor of Drop Dead Phenotype

12. *fbn1-fibrillin 1*

13. *mua-3- muscle attachment abnormal-3*

14. cbEGF-Calcium Binding Epidermal Growth Factor

15. LTBP- Latent TGFβ binding proteins

ABSTRACT

DEVELOPING A C.ELEGANS MODEL OF MARFAN SYNDROME
By Pauline Effie Andreas Fotopoulos M.S.

A thesis submitted in partial fulfillment of the requirements for the
degree of Master of Science in Biochemistry and Molecular Biology at Virginia Commonwealth University.

Virginia Commonwealth University, 2014.

Major Director: Young You, Department of Biochemistry and Molecular Biology

Marfan Syndrome (MFS) is one of the most common monogenic diseases and affects approximately 1 in 5,000 individuals worldwide. The syndrome is characterized by elongated extremities, tall stature, slender frame, and cardiac, and vision abnormalities due to severe connective tissue defects. It is caused by mutations in the *fbn1* gene, which encodes an extracellular matrix glycoprotein, and is required for proper cardiac and skeletal development and for sequestration of TGFβ (transforming growth factor beta) and BMP (bone morphogenetic protein) within the extracellular matrix (ECM).

The primary objective of this study was to establish a *C.elegans* MFS model and use this model to determine which genes interact with a *C.elegans fbn1* homolog, MUA-3 and ascertain the role of metabolic rate in the development of MFS pathology. We isolated a temperature

sensitive mutant of *mua-3*, a *fbn1* homolog. We found that at the fourth larval molt, when animals shed the exoskeleton and rebuild a new one, the mutants die due to extensive mechanical stress in connective tissue shown as fragmented internal structures. Using this mutant, an unbiased forward genetic screen to isolate the genetic interactors of the fibrillin gene homolog, was completed. A collagen gene, that has been implicated to genetically interact with a bone morphogenetic protein (BMP), was isolated. This suggests that *mua-3(uy19)* may interact with genes involved in TGFβ regulation during the L4 molt and that fibrillin-1, TGF-β, and metalloproteases may act in-concert to modulate TGFβ availability and connective tissue integrity in *C. elegans*.

In addition, we found that two independent mutations of *mua-3* show temperature-sensitive phenotypes. Based on this result, we propose that increase of temperature aggravates the phenotype potentially due to increased metabolism. This hypothesis, if correct, will suggest a potential connection between metabolic rate and severity of MFS pathology.

1. Introduction

1.1 Marfan Syndrome

Marfan syndrome (MFS) is an autosomal dominant connective tissue disorder and among the most common monogenic diseases worldwide(Gao et al. 2010). The syndrome affects approximately 1 in 5000 individuals worldwide and occurs with high penetrance but notable inter- and intra-familial variation(Gao et al. 2010). Manifestations of the disease typically involve effects on the ocular, skeletal, and cardiovascular systems(Ramirez & Dietz 2007). Patients exhibit connective tissue and skeletal defects such as tall habitus, elongated extremities, joint hypermobility, scoliosis, striae, and chest wall deformities(Ramirez & Dietz 2007) (Figure 1)(Joyce 2011). Cardiovascular manifestations range in severity from mitral valve prolapse, progressive aortic root enlargement, to acute aortic dissection(Ramirez & Dietz 2007).Ocular symptoms include myopia, retinal detachment, lens subluxation, and ectopia lentis (malpositioning of the lens with typical bilateral presentation) (Gao et al. 2010). MFS is caused by mutations in the *fbn1*gene(Ramirez & Dietz 2007).

Figure 1: Individual with MFS, shown here undergoing a clinical diagnostic test(Joyce 2011).

(Joyce 2011)

1.2 Fibrillin-1

MFS results from mutations in the *fbn1* gene which encodes an extracellular matrix (ECM) glycoprotein, fibrillin-1. Fibrillin-1 has a proline rich composition bias and is composed of 47 Epidermal Growth Factor (EGF)-like domains, 43 of which are able to bind to calcium (Figure 2)(Ramirez & Dietz 2007). These calcium binding EGF-like domains serve as the structural foundation for extracellular microfibrils in both elastic and non-elastic connective tissue throughout the organism(Zangwill et al. 2006). In addition, the protein contains nine transforming growth factor beta (TGF-β) binding domains (8scy/TB) which are highly homologous to latent TGFβ binding proteins(Gao et al. 2010). The N-terminus is considered a high affinity nonspecific binding site for all TGFβ family members(Sengle et al. 2008). Once secreted FBN-1 monomers aggregate and form beaded structures, which form macro-aggregates, microfibrils. Microfibrils may exist independently or become embedded in elastic fibers during embryogenesis (Figure 2) (Ramirez & Dietz 2007). Within these microfibrils, the functional role of FBN-1 is to sequester TGFβ and Bone Morphogenic Proteins (BMPs) in the ECM prior to activation.

Figure 2: Organization and aggregation of fibrillin-1 proteins following secretion. A. Representative structure of fibrillin-1 including TGFβ binding domains and calcium binding Epidermal Growth Factor-like domains. B. Fibrillin-1 monomers develop into beaded structures that form macro-aggregates and constitute microfibrils which may exist independently or become incorporated into elastic fibers during embryogenesis. cbEGF-Calcium Binding Epidermal Growth Factor ; TB-Transforming Growth Factor β Binding Domain; Cys-cysteine . Image adapted from (Ramirez & Dietz 2007).

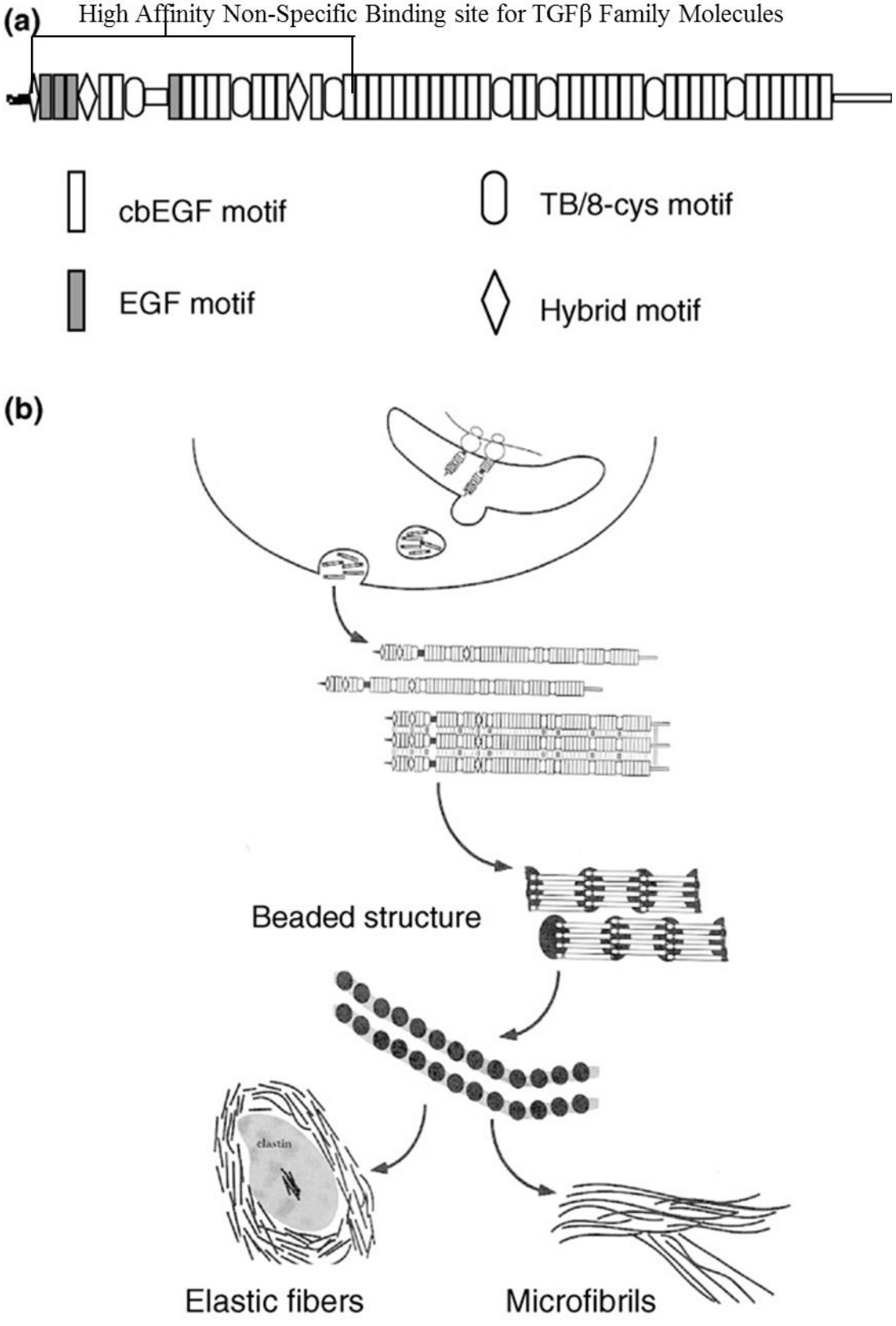

(Ramirez & Dietz 2007)

Over 1750 mutations in *fbn1* are known to result in MFS and related disorders with over 1000 mutations associated with MFS alone(Horiguchi et al. 2012; Gao et al. 2010). Frequently, these mutations result from premature termination codons or in-frame deletions(Gao et al. 2010). *De novo* mutations in FBN-1 account for 25% of MFS cases(Ramirez & Dietz 2007). FBN-1 is involved in cardiac development and skeletal development(Nistala et al. 2010). Skeletal development is affected by the modulation of osteoblast formation through TGFβ regulation(Nistala et al. 2010). FBN-1 is critical for modulating the TGFβ signal because it sequesters TGFβ and BMP (bone morphogenic protein) within the extracellular matrix (ECM) (Nistala et al. 2010) (Figure 3)(Handford 2012).

Figure 3: Latent TGFβ complex shown bound to N-terminal region of fibrillin-1. TGFβ-Transforming Growth Factor β; LTBP-Latent TGFβ Binding Protein. Image Adapted from (Handford 2012)

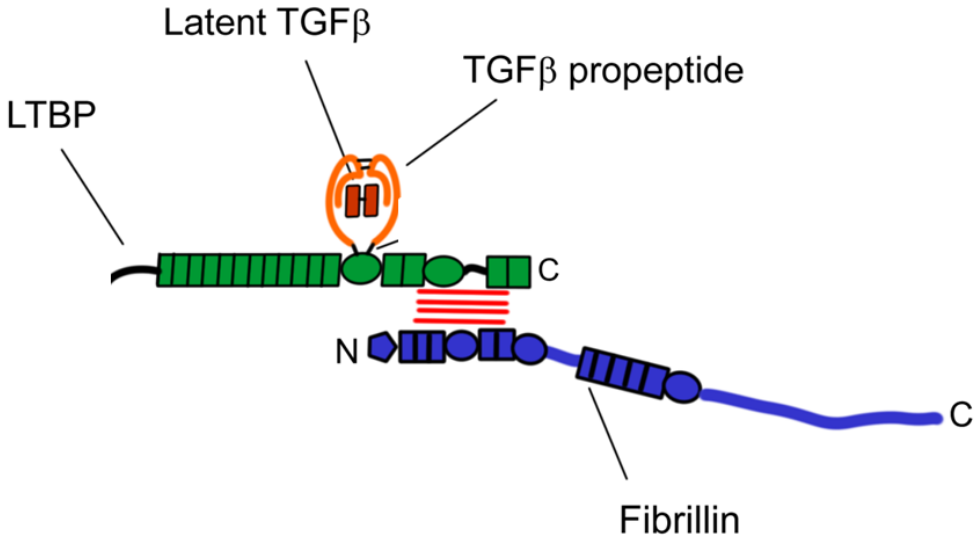

(Handford 2012)

1.3 TGF-β

TGF- β is involved in cell proliferation, differentiation, apoptosis, migration, immunity, angiogenesis, ECM production(Le Goff & Cormier-Daire 2012) and development (vascular, cardiac, lung, urogenital, craniofacial)(Massagué et al. 2000). An overview of TGFβ activation is given in Figure 4(Horiguchi et al. 2012). Synthesized as a preproprotein, monomers dimerize via a disulfide bond, resulting in a pro TGFβ homodimer(Horiguchi et al. 2012). A latency associated peptide (LAP) is non-covalently associated with TGF-β, forming the small latent complex (SLC)(Horiguchi et al. 2012). LAP imparts latency by preventing the growth factor domain from binding to its receptor or by inducing a conformational change of the growth factor domain that inhibits receptor binding(Sengle et al. 2008). The homodimer binds to a Latent TGFβ binding protein (LTBP) through a disulfide bond(Horiguchi et al. 2012). Furin convertase then cleaves the TGFβ prodimer to the mature TGF-β(Horiguchi et al. 2012). The large latent complex (LLC) forms when LAP, binds to the 8 cysteine motif TGFβ binding domain of LTBPs through a disulfide bond(Horiguchi et al. 2012). Latent TGFβ may either be secreted as SLC (LAP and TGF-β) or as LLC (SLC bound to LTBP) from the endoplasmic reticulum(Horiguchi et al. 2012; Le Goff & Cormier-Daire 2012). Soluble SLCs are unbound to LTBPs and not properly activated or targeted to the ECM, therefore the formation of the LLC is critical to TGFβ signaling(Horiguchi et al. 2012). LTPBs will target the entire LLC complex to the ECM by binding to the N terminal region containing TGFβ binding sites on FBN-1, which may be embedded in elastic microfibrils(Horiguchi et al. 2012). Sequestration of the latent TGFβ complex prevents untimely TGFβ activation and excess signaling.

Figure 4: TGFβ processing within the endoplasmic reticulum, secretion, and subsequent sequestration within the ECM. 1) TGFβ monomers form homodimers. 2) TGFβ binds LAP and LTBP. 3) Furin convertase cleaves the proportion of TGFβ to form the mature TGF-β. 4) LLC, which includes TGF-β, LAP, and LTBP are secreted from the ER. 5) LTBP binds FBN-1 in microfibrils and is targeted to the ECM. Figure adapted from (Horiguchi et al. 2012).

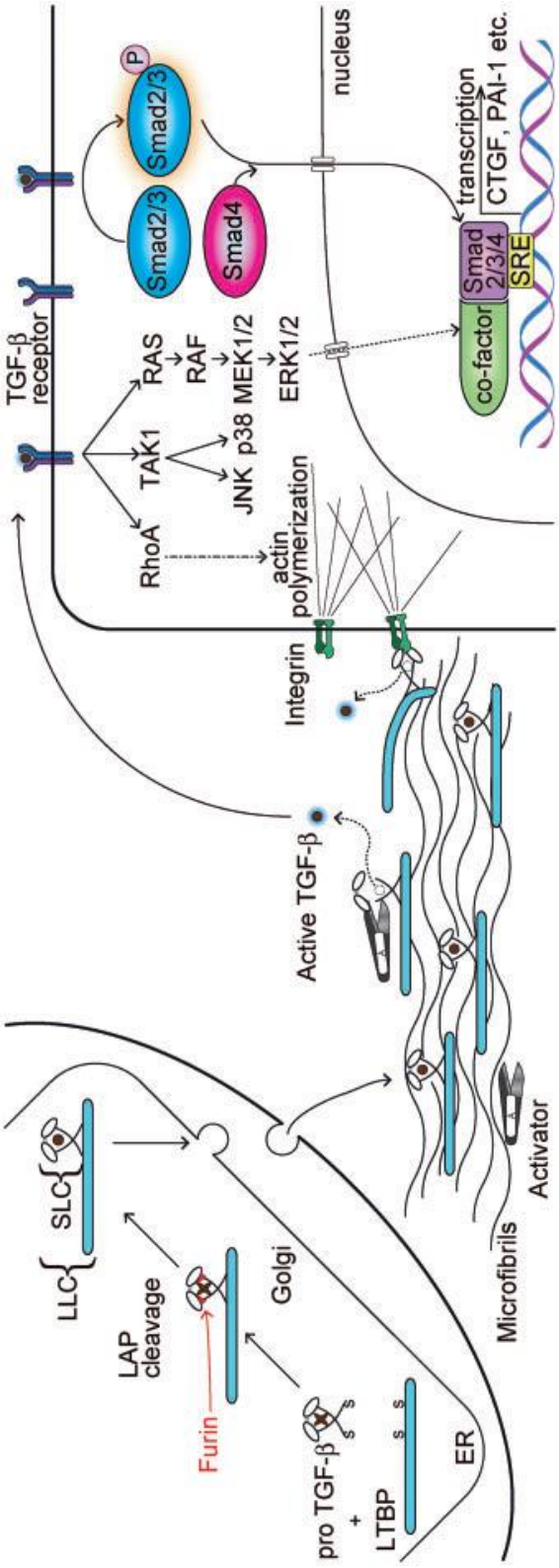

(Horiguchi et al. 2012)

TGFβ activation occurs following the release of the LLC from microfibrils and the ECM (Le Goff & Cormier-Daire 2012). TGFβ is released from the LLC through latent complex conformational modification or by LAP / LTBP degradation (Horiguchi et al. 2012). All activation mechanisms target LAP (Le Goff & Cormier-Daire 2012) although they may differ by cell type. Latent TGFβ can be activated by proteases, thrombospondin-1, reactive oxygen species, and integrins(Horiguchi et al. 2012). BMP-1, a metalloproteinase cleaves LTBP1 at two sites in the hinge region which releases SLC (Le Goff & Cormier-Daire 2012) and degrade LAP directly (Horiguchi et al. 2012), leading to TGFβ activation. Active TGFβ binds to its serine/threonine transmembrane receptors which in turn phosphorylate SMADs. SMADs return to the nucleus, accumulate, and regulate the transcription of genes(Ramirez & Dietz 2007).

1.4 FBN-1 and TGFβ in Marfan pathology

Proteolytic cleavage can degrade the ECM, resulting in the release of LLC, and activation of latent TGFβ (Horiguchi et al. 2012). Within the ECM, one function of FBN-1 is to sequester TGFβ containing complexes to regulate TGFβ signaling. TGFβ complexes are released from FBN-1 when FBN-1 is proteolytically degraded or LTBP is cleaved. Normal individuals have sufficient FBN-1 rich microfibrils to sequester TGFβ prevent excess TGFβ activation. During proteolysis fibrillins become fragmented, and these fragments will interact with the N terminus of FBN-1. The FBN-1 fragment and microfibril interaction is followed by displacement of LTBP and subsequent release of LLC (Le Goff & Cormier-Daire 2012). Proteolysis of fibrillin rich microfibrils induces the expression of metalloproteinases and macrophage chemotaxis leading to aortic aneurysm progression(Guo et al. 2006; Booms et al. 2005). Structural defects in microfibrils, such as FBN-1 defects, result in a failure to sequester latent complexes, leading to

excess TGFβ activation and a subsequent increase in TGFβ signaling mediated by SMADs(Le Goff & Cormier-Daire 2012; Ramirez & Dietz 2007; De Backer et al. 2009) (Figure 5. 2) (Ramirez & Dietz 2007) . One of the primary functions of FBN-1 is to control TGFβ signal intensity (Ramirez & Dietz 2007). In patients with MFS, defects in FBN-1 lead to excess TGFB signaling, which results in the pleiotropic manifestations of disease (Figure 5)(Ramirez & Dietz 2007).

Currently MFS is treated with β-adrenergic blockers to lower heart rate and slow aortic growth. However, this only ameliorates the deleterious symptoms of progressive aortic root enlargement and aortic dissection(Ramirez & Dietz 2007). To address this problem other medications have been developed, such as losartan. Losartan is an angiotensin II receptor blocker(De Backer et al. 2009), which targets a cause of the disorder, by lowering TGFβ levels, reducing the expression of TGFβ activators and TGFβ receptors(Ramirez & Dietz 2007). Although it is clear that the relationship between FBN-1 and TGFβ contributes to the development of MFS, questions remain regarding the underlying mechanism. To further delineate how FBN-1 mutations modulate TGFβ signaling leading to the MFS phenotype, a model system can readily be genetically manipulated was necessary.

Figure 5: 1) Normal TGFβ sequestration and regulation by FBN-1. 2) Reduced microfibril formation due to FBN-1 mutations. Improper FBN-1 deposition allows the release of LLC and the subsequent activation of TGF-β. Once activated TGFβ binds to its serine/ threonine transmembrane receptor and mediates TGFβ induced transcriptional responses. TGFβ dysregulation and excess activation mediates the phenotypic outcomes associated with MFS pathology. Figure adapted from (Ramirez & Dietz 2007).

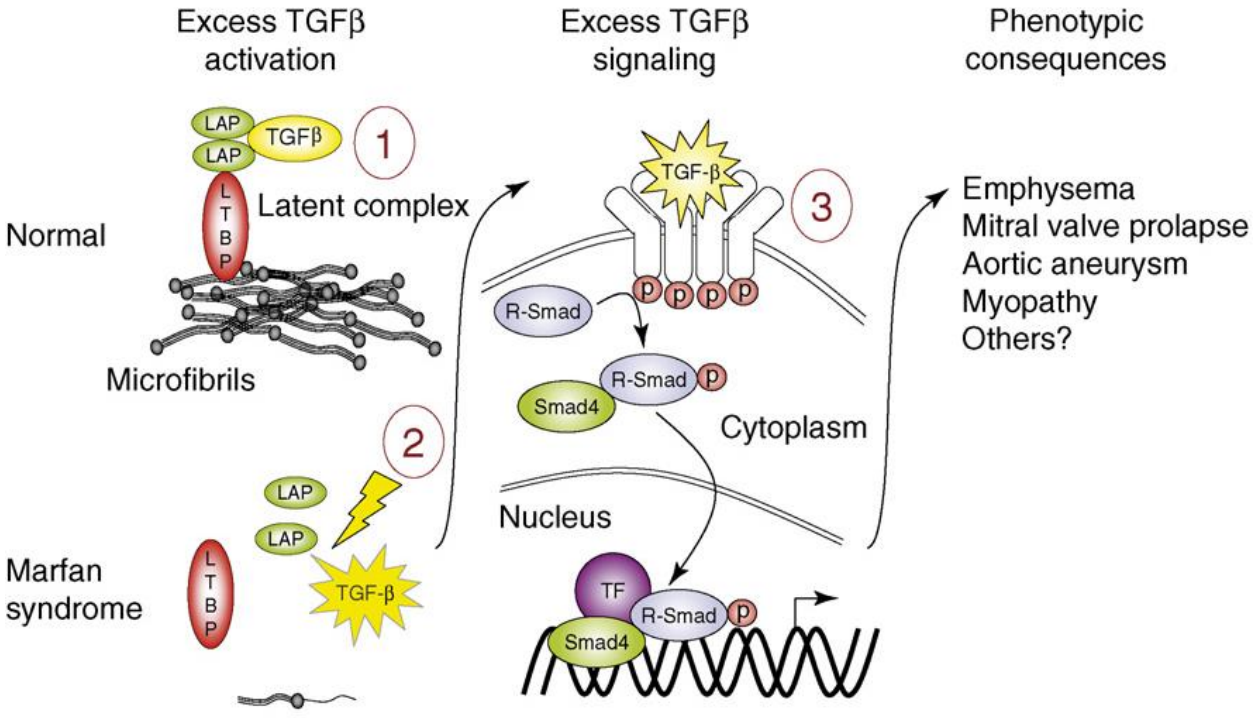

(Ramirez & Dietz 2007)

1.5 Developing a MFS Model in *C.elegans*

C.elegans is a nematode that has long served as a model system for studying development, neurobiology, and behavioral biology(Riddle DL, Blumenthal T, Meyer BJ, et al. 1997; Avery 2007). Most importantly, considerable conservation exists between this multicellular organism and humans, 35% of *C.elegans* genes have human homologs(Riddle DL, Blumenthal T, Meyer BJ, et al. 1997; Avery 2007). The complete cell lineage is well characterized and genes can be altered, removed, or added to the genome. Self-fertilization and cross-fertilization can also be manipulated(Riddle DL, Blumenthal T, Meyer BJ, et al. 1997; Avery 2007). The nematode has a short life cycle (Figure 6)(Altun, Z. F. and Hall 2005), small size, is transparent, easily cultivated in the laboratory, and generates 300-350 progeny(Riddle DL, Blumenthal T, Meyer BJ, et al. 1997; Avery 2007). Forward and reverse genetic screens aim to determine the genetic basis of a phenotype and the phenotype which results from a specific sequence, respectively. These screens can be employed to determine potential genetic and protein interactions(Riddle DL, Blumenthal T, Meyer BJ, et al. 1997; Avery 2007).Furthermore, we show that the molecular pathways and potential pathophysiology underlying MFS is conserved between mammals and worms.

Figure6: *C.elegans* life cycle, including the duration of each life cycle stage at 25°C. Figure adapted from (Altun, Z. F. and Hall 2005).

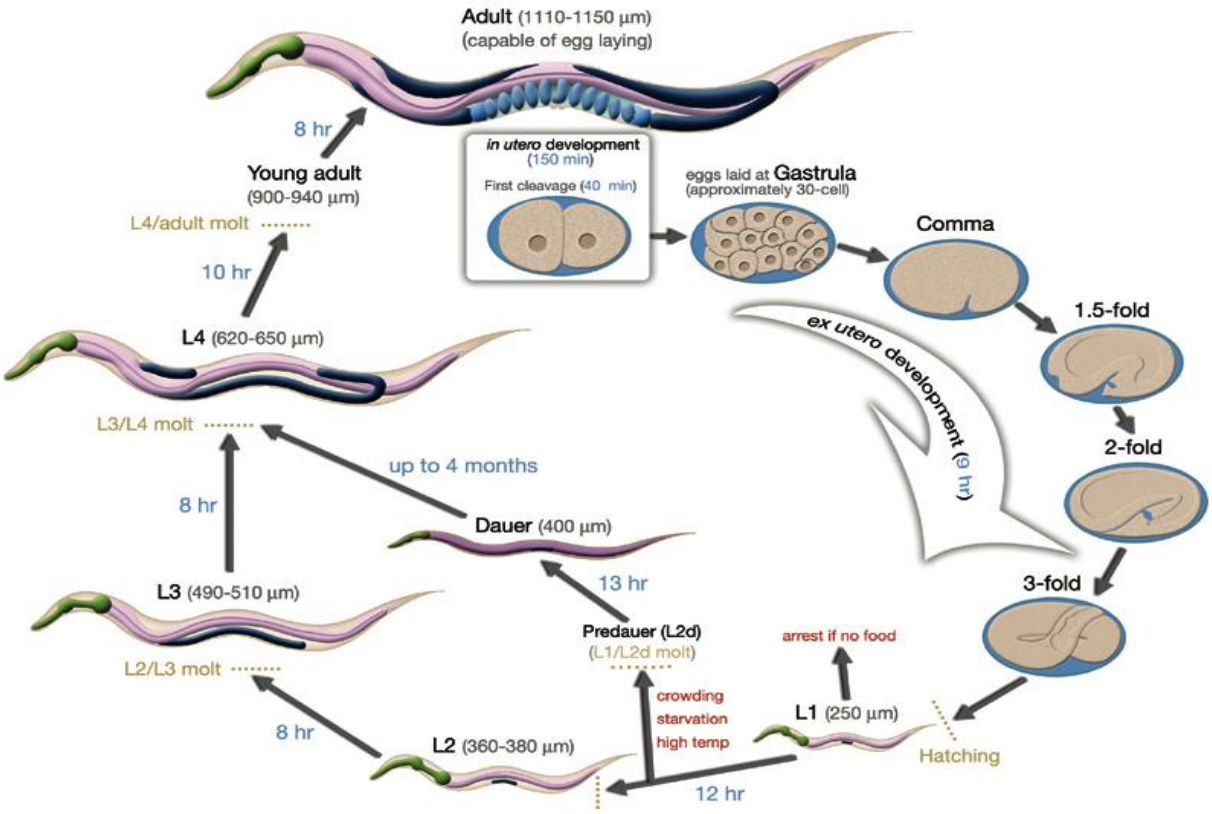

(Altun, Z. F. and Hall 2005)

1.6 Conserved Pathways and Homologs of MFS

In *C. elegans*, *fbn-1* and *mua-3* are both homologs of human FBN-1 (Table 1)(Riddle DL, Blumenthal T, Meyer BJ, et al. 1997; Bercher 2001; Frand et al. 2005; Culetto & Sattelle 2000). MUA-3, encoded by the *muscle attachment abnormal-3 (mua-3) gene,* localizes to hypodermal cells in which body wall muscle adhesion occurs and sites of transhypodermal stress (Bercher 2001). *mua-3,* is needed during postembryonic adhesion of the hypodermis to the cuticle(Bercher 2001). A defect in *mua-3* is characterized by progressive muscle detachment throughout larval development (Bercher 2001). *Fbn-1* is required for proper molting, specifically during the L3/L4 molt and L4/young adult molt(Frand et al. 2005). Complete knockout of *mua-3* is lethal, while *fbn-1* knockdown mutants exhibit molting defects, sterility, larval lethality, slow growth, and lay dead eggs(Riddle DL, Blumenthal T, Meyer BJ, et al. 1997; Bercher 2001; Frand et al. 2005; Culetto & Sattelle 2000). This suggests that although both genes are homologous to *fbn1* in humans, these genes are not functionally redundant. Mutations in *fbn-1* and *mua-3* genes cause molting defects that can be attributed to defects in connective tissue(Bercher 2001). This demonstrates that *C. elegans* fibrillin genes have a conserved role in maintaining connective tissue integrity in both humans and *C.elegans.* The defects in molting that these *C.elegans* mutants show, suggest that the mechanical strain of molting (shedding and rebuilding the exoskeleton) could mimic MFS pathology.

Table 1: BLAST summary of human *fbn1* homologs in *C.elegans.* The *C.elegans, fbn-1* covers a greater sequence range of human *fbn1,* than *mua-3*. *mua-3* exhibits a higher E-value and total score. Both *fbn-1* and *mua-3* are homologs fibrillin-1. (Altschul SF1, Gish W, Miller W, Myers EW 1990)

Table 1: Human FBN1 homologs in *C. elegans*

Description	Max Score	Total Score	Query cover	E value	Max identity
C.elegans **MUA-3 isoform b**	**181**	**1854**	**86%**	**5e-45**	**32%**
C.elegans **MUA-3 isoform a**	**179**	**2421**	**86%**	**2e-44**	**45%**
C.elegans **FBN-1 isoform h**	**171**	**2375**	**91%**	**4e-42**	**45%**

(Altschul SF1, Gish W, Miller W, Myers EW 1990)

Although a *mua-3/fbn-1* and TGFβ relationship similar to their human counterparts has not been established, interestingly in *C. elegans*, most genes that regulate body size are components of the TGFβ pathway(You et al. 2008; van der Linden et al. 2008), (Avery & You 2012; Lee et al. 2012). A homolog of human Bone Morphogenic Protein-1, a tolloid-like gene responsible for TGFβ activation, is *dpy-31*(Novelli et al. 2004). *dpy-31* is essential to cuticle formation, embryonic/larval development at 25°C, and is expressed throughout the organism(Novelli et al. 2004). The effects of mutations in *dpy-31* can be suppressed by gain of function mutations in *dpy-17*, a cuticle collagen required for posterior outgrowth(Riddle DL, Blumenthal T, Meyer BJ, et al. 1997; Buechner 2002; Brenner 1974; Novelli et al. 2004).

1.7 Temperature Sensitivity

Forward genetic screens can be used to isolate suppressors of temperature dependent phenotypes. Strains which exhibit temperature sensitivity include the *muscle attachment abnormal*-3 (*mua-3*) gene, a homolog to *fbn1* in humans. *mua-3* mutant alleles can exhibit connective tissue and molting defects similar to the MFS phenotype (Figure 7). A *mua-3(uy19),* 131 amino acid in-frame deletion mutant and a *mua-3 (rh195)* single base pair substitution (missense) mutant were obtained. At the L4 molt, the stage prior to reproductive adulthood, *mua-3 (uy19)* and an alternate allele, *mua-3 (rh195)* exhibit death and sterility phenotypes, respectively, at restrictive temperatures (Figure 7). However at permissive temperatures both mutant strains appear normal. The lethality and sterility phenotypes result from molting defects at the L4 stage. The molting defects may be attributed to a connective tissue defect. Worms exhibit internal organ misplacement, connective tissue detachment, or gonadal detachment. These symptoms mimic those observed in MFS. Clinical manifestations of MFS appear to be

dependent on developmental stage, particularly in adolescence for humans, similar to the L4 stage in worms which precedes reproductive adulthood.

Figure 7: A. Differential Interference Contrast (DIC) light microscopy image of *mua-3(uy19)* mutant at 20°C in the L4 stage. Connective tissue defect of *mua-3 (uy19)* mutant grown at a restrictive temperature. B. DIC image of *mua-3(rh195)* mutant at 25°C in L4 stage. Connective tissue defect of *mua-3 (rh195)* mutant grown at a restrictive temperature. Connective tissue defects of *mua-3* mutant alleles including connective tissue detachment and internal organ misplacement are depicted. Images courtesy of Inwahn Lee.

A

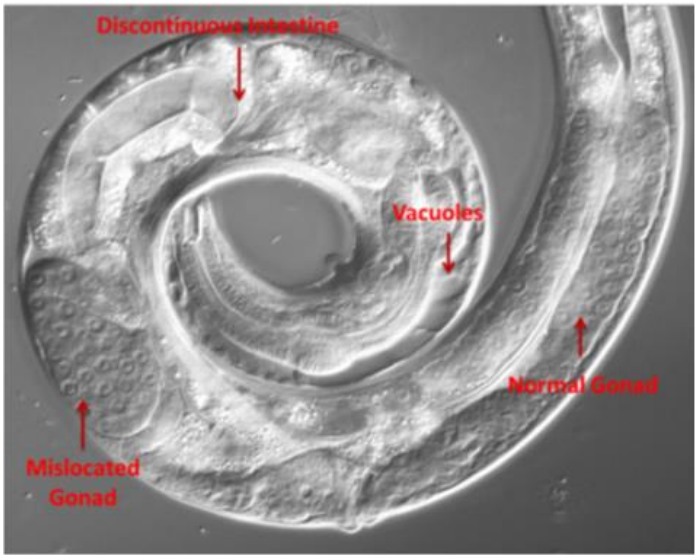
Discontinuous Intestine
Vacuoles
Normal Gonad
Mislocated Gonad

B

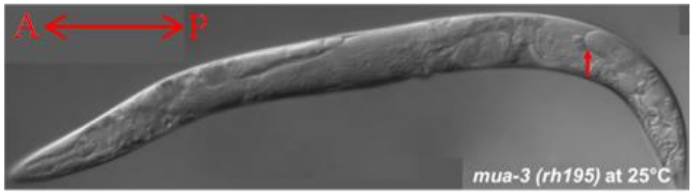
A
P
mua-3 (rh195) at 25°C

Since considerable conservation in the gene and phenotype exists, we aimed to establish a *C.elegans* MFS model and determine how *mua-3* contributes to the Marfanoid phenotype via its protein interaction network. With the enriched resources, a *C. elegans* model for MFS can potentially be used to develop other effective drugs to treat MFS.

1.8 Implications of Forward Genetic Screens

Temperature variation experiments were used to characterize the phenotypes of the *mua-3 (uy19)* and *(rh195)* mutant alleles. The temperature sensitive nature of the *mua-3 (uy19)* lethality phenotype permitted the use of an unbiased forward genetic mutant screen to isolate suppressors of *mua-3(uy19)* lethality. Several suppressors were isolated, the majority of which had smaller body size and slower growth rate. Therefore our results provide the first genetic evidence at the organismal level that the fibrillin-1 gene and the TGFβ pathway may interact.

Upon complementation testing, we identified *dpy-17* mutations as suppressors of the *mua-3(uy19)* phenotype from separate genetic screens. This validates our result that *dpy-17* suppresses the lethality phenotype of *mua-3(uy19)* and therefore suggests that DPY-17 and MUA-3 interact genetically during molting.

In this study, the primary aims were to establish a *C.elegans* MFS model and use this model to delineate the protein interaction network that contributes to the Marfanoid phenotype. Using *C.elegans* as a model for studying MFS, we characterized the temperature sensitive phenotype of *mua-3(uy19)* and used this characterization to identify genetic interactors of MUA-3. One interactor, DPY-17, is known to genetically interact with DPY-31, a BMP-1 homolog(Novelli et al. 2004). Together, our results suggest that fibrillin-1, TGF-β, and metalloproteases may act in-concert to modulate TGFβ availability and connective tissue integrity in *C. elegans*(Figure 8). These results also show the molecular conservation among

known genetic causes for Marfan or Marfan-related syndromes. Furthermore, this suggests that the molting process in *C. elegans* can be used to study Marfan pathology.

Figure 8: Potential interactions indirectly linking *mua-3(uy19)* to TGFβ pathway involvement.

Interactions

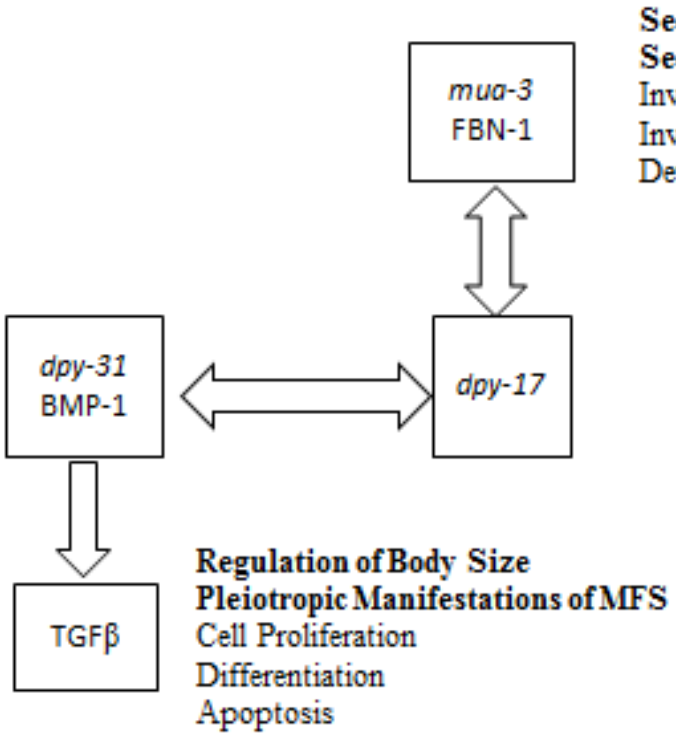

Sequesters BMP
Sequesters TGFB
Involved in Heart Development
Involved in Skeletal Development

Regulation of Body Size
Pleiotropic Manifestations of MFS
Cell Proliferation
Differentiation
Apoptosis

2. RESULTS

2.1 characterization of *mua-3 (uy19) and mua-3 (rh195)* mutants

To establish *C. elegans* as model for MFS it was necessary to thoroughly characterize the newly discovered *mua-3* mutant alleles and phenotypes. Genome sequencing confirmed mutations in *mua-3*. One allele *mua-3(uy19)* contained a 131amino acid in-frame deletion and a separate allele *mua-3 (rh195)* possessed a single base pair substitution resulting in a missense mutation.

2.2 mua-3(uy19) and *mua-3(rh195)* mutants appear larger than wild-type

Up-regulation of genes and products within the TGFβ pathway typically confers a larger phenotype and is implicated in MFS pathology. To establish the *mua-3* mutant as a model for MFS, we aimed to determine the characteristic lengths of TGFβ mutants and compare these measurements with length measurements of *mua-3* mutants. Quantitative measurements of worm body length for *mua-3(uy19) (YJ35)*, wild type (Bristol, N2), *dbl-1* (ctIs40) (BW1940), *lon-1* (*e185) (CB185), lon-2* (*e678*) (CB678), *mua-3 (rh195)(OT136)* were taken (Figure 9). Although *mua-3(uy19)* and *mua-3(rh195)* (data not shown) appear larger than wild type, results from experiments with separate procedures were inconsistent and inconclusive. Although, TGFβ mutant strains tended to larger than wild-type, there were no statistically significant differences among the strains. The inconsistency observed may be attributed in part to technical difficulties resulting from the nature of the connective tissue phenotype. The inherent weakness of the mutant strains' connective tissue and the use of sodium azide to fix the worms onto agar slides, may have caused an exaggerated contraction, altering the length of the mutant. Demonstrating that *mua-3*mutants and mutants with TGFβ upregulation are larger in length would further characterize *mua-3* mutants as Marfan-like and further establish the observed *mua-3* phenotype as a model for MFS.

Figure 9: Averaged length of *mua-3(uy19)(YJ35), wild type (N2), dbl-1 (ctIs40)(BW1940), lon-1 (e185)(CB185),* and *lon-2 (e678)(CB678)* strains at 72 hours post collection at L4 stage. An average of 5 worms/strain are represented in the graph (n=2). This data was generated with DIC microscopy. None of the length measurements are significantly different.

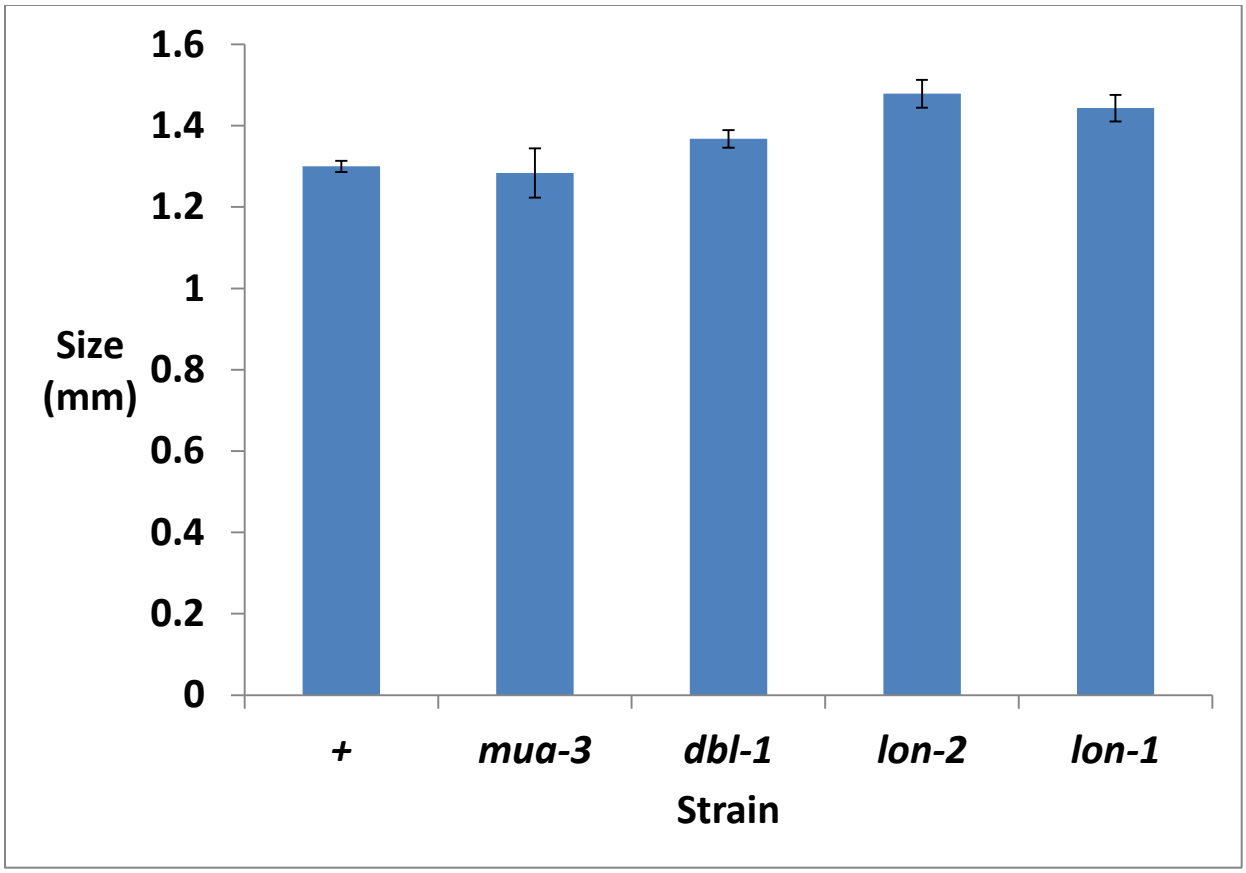
1.6
1.4
1.2
1
0.8
0.6
0.4
0.2
0
Size (mm)
+
mua-3
dbl-1
lon-2
lon-1
Strain

2.3 mua-3 mutants are molting defective and experience higher death rates via connective tissue defects during the L4 stage than wild type

Molting defects due to connective tissue detachment are pictured (Figures 7A and 7B). *mua-3 (rh195)* mutants exhibit gonadal detachment while *mua-3 (uy19)* mutants exhibit internal organ misplacement and connective tissue detachment. Temperature variation and time course experiments were performed with *mua-3(uy19)* and wild type strains to identify the stage at which *mua-3(uy19)* deaths occur and determine whether an increase in temperature increases *mua-3(uy19)* lethality via connective tissue defect (Figure 7A). These results provide evidence that lethality occurs during the L4 stage, the stage prior to reproductively active adulthood, at restrictive temperatures (Figure 10 A and B). At the L1, L2, and L3 stages there were no deaths observed and only a few deaths were observed at stages past L4. The time required for worms to mature from L1 to L4 at 25°C is approximately 30 hours. The L4 stage will last for at least 6 hours. At 20°C, maturation from L1 to L4 requires about 38 hours, while at 15°C maturation requires 63 hours. The L4 stage at 20°C and 25°C will last for approximately 9 hours. The majority of death occurred within the L4 stage timeframe designated above, for 15°C, 20°C, and 25°C respectively.

At the permissive temperature, 15°C, *mua-3* and wild type worms at the L4 stage had a death rate of, nearly zero and exhibited no molting defects (Figure 10 C). However, at restrictive temperatures, 20°C and 25°C, there was a statistically significant difference between deaths observed in wild type and *mua-3* strains. This provides evidence that lethality occurs only at restrictive temperatures (20°C and 25°C). Furthermore, lethality was enhanced at 25°C in comparison to 20°C.

The difference in survival of *mua-3* mutants between permissive and restrictive temperatures indicates that connective tissue defects and lethality increase with increasing temperatures. The results of the temperature variation and time course experiments support the assertion that it is specifically at the L4 stage that *mua-3* deaths occur. At higher temperatures, 25°C, the mechanical strain of molting increases, metabolic rate accelerates, and protein folding may be affected. Higher temperatures correspond to increased lethality and therefore may be attributable to an increase in metabolic rate or improper folding of the protein. Characterization of the *mua-3* mutant phenotype allowed us to perform an unbiased forward genetic screen in which we could isolate suppressors of the connective tissue defect, lethality phenotype.

Figure 10: A. Time course of percent survival observed for *mua-3* and wild type strains at 20°C. n=6 worms/treatment; average of data at each time point is shown. The difference is statistically significant at $P < 0.01$. B. Time course of percent survival observed for *mua-3* and wild type strains at 25°C. n=8 worms/treatment; average of data at each time point is shown. The difference is statistically significant at $P < 0.01$. C. Time course of percent survival observed for *mua-3* and wild type strains at 15°C. n=6 worms/treatment; average of data at each time point is shown. The difference is not statistically significant.

A

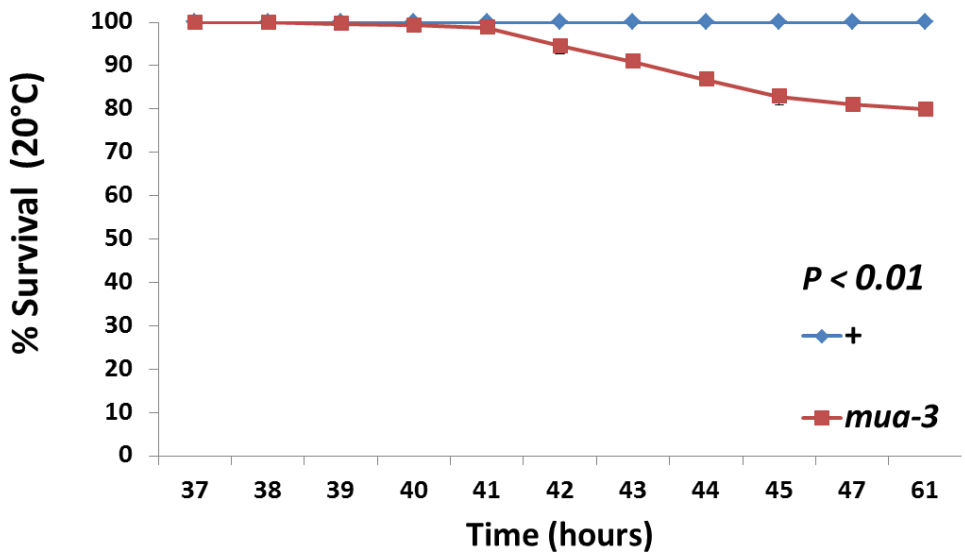
% Survival (20°C)
100
90
80
70
60
50
40
30
20
10
0
37
38
39
40
41
42
43
44
45
47
61
Time (hours)
P < 0.01
+
mua-3

B

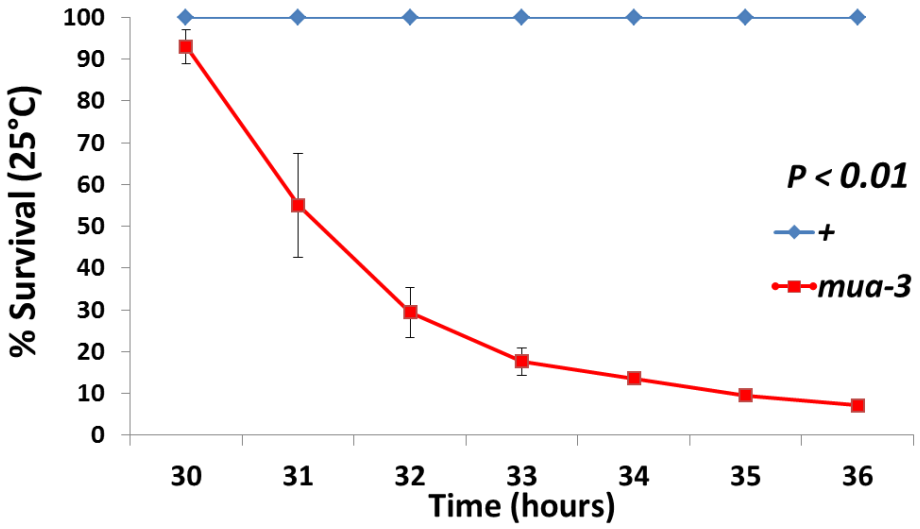
% Survival (25°C)
100
90
80
70
60
50
40
30
20
10
0
30
31
32
33
34
35
36
Time (hours)
P < 0.01
+
mua-3

C

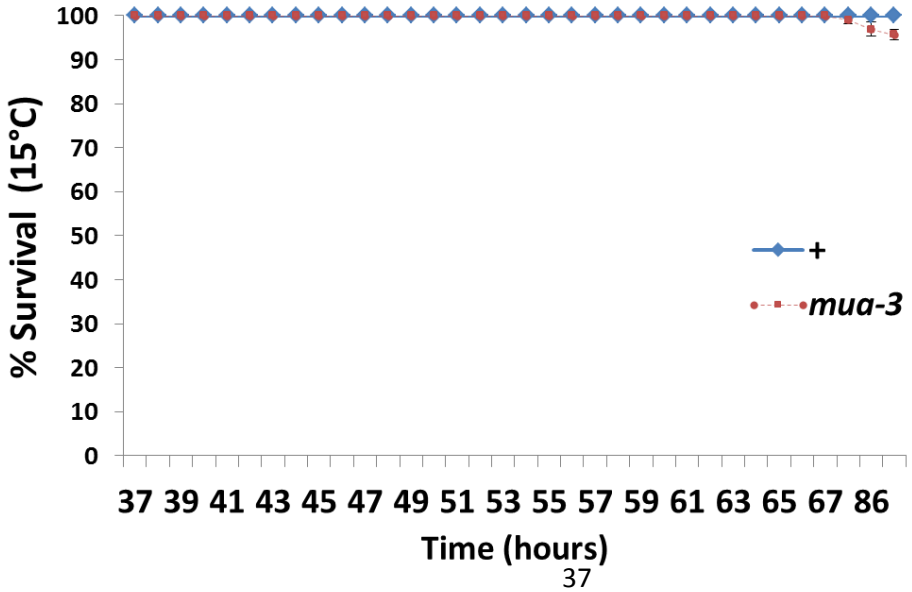
% Survival (15°C)
100
90
80
70
60
50
40
30
20
10
0
37 39 41 43 45 47 49 51 53 55 57 59 61 63 65 67 86
Time (hours)
+
mua-3

Table 2: 841 fold decrease in progeny from wild type to *mua-3(rh195)(OT136)* at the 25°C, restrictive temperature. The graph represents an average of the total number of progeny produced by worms at 25°C (n=10). The difference is statistically significant at $P < 0.001$.

Strain	Number of Progeny
+	1682
mua-3	2

2.4 mua-3(rh195) mutants experienced significantly higher sterility rates at the restrictive temperature than wild type

To establish *C. elegans* as model for MFS, it was necessary to characterize the phenotype associated with mutations in *mua-3(rh195).* At the permissive temperature, *20*°C, there is no noticeable difference in the number of progeny produced by the *mua-3 (rh195)* mutant and wild-type worms. However, *mua-3(rh195)* experienced much higher connective tissue defect and sterility rates than wild type when grown at the restrictive temperature, 25°C. Specifically, gonadal detachment occurs in *mua-3(rh195)* mutants at 25°C. When grown at the restrictive temperature the rate of sterility for *mua-3* mutants nears 100% (Table 2). Evidence of the rate of sterility for this mutant allele is provided by data in which total offspring of individual worms was counted. We have shown that the difference in the number of progeny produced by wild type and *mua-3 (rh195)* worms at the restrictive temperature, 25 °C, is statistically significant. The 841 fold decrease in progeny from wild type to *mua-3(rh195)* at restrictive temperatures (Table 2) indicates that *mua-3(rh195)* mutants are sterile at restrictive temperatures.

2.5 Suppressors of the MFS phenotype of *mua-3(uy19)* have been discovered

To identify suppressors of the *mua-3(uy19)* MFS phenotype, an unbiased forward genetic F2 screen was performed using Ethyl Methyl Sulfonate (EMS) mutagenesis. It was determined that the lethality observed at the 25°C, restrictive temperature, was far more severe than 20°C and would serve as a better treatment for screening the temperature sensitive mutants. A secondary temperature screen at 25°C was performed to identify and remove sterile (worms that produced no progeny) and escaper worms (worms that produced non-viable progeny). Approximately 20, F2 potential suppressors were isolated (Table 3). The trend among

suppressors of *mua-3(uy19)* lethality phenotype is that of shortened body length, slower growth, and slower egg laying (Table 3). These experiments allowed us to determine potential *mua-3(uy19)* interactors and begin to form a picture of how *mua-3(uy19)* may be involved in TGFβ regulation and therefore MFS pathology. It provides the foundation upon which we may search for and establish a mechanism by which MFS progresses.

Table 3: Characterization of isolated suppressors of the *mua-3(uy19)* lethality, MFS-like, phenotype (Suppressor Of Drop Dead, SODD). SODD 1-SODD 15 includes suppressors isolated from the first screen. SODDD 16-SODD 27 includes suppressors isolated from the second screen.

SODD	Extreme Short Length	Short Length	Wild-type length	Long Length	Extreme Long Length	Disproportioned	Thin	Fat	Hooked
1		x					x		x
3			x						
4							x		
5			x						x
6		x					x		
7		x					x		
8		x					x		
9		x					x		
10		x					x		x
11	x					x			
12	x					x			
14	x					x			
15		x					x		
16		x					x		
17		x					x		x
18	x					x			
19	x					x			
20			x				x		
21					x		x		
22		x					x		
23	x					x			
24			x	x				x	
25			x						
26			x	x					
27			x	x					

SODD	Pale	Dark	Slow Growth	Slow - abnormal Motility	Bands	Crumpled-Misplaced structures	Agitated Behavior	Blister	Round
1	x								
3					x	x			
4									
5							x		
6	x								
7	x			x					
8	x								x
9		x							
10									x
11		x	x	x					x
12		x	x	x					
14		x	x	x					
15				x					
16			x	x					
17	x		x	x				x	
18									
19		x							
20					x				
21					x				
22	x		x	x	x				
23		x							
24									
25									
26		x							
27		x							

Figure 11: SODDs rescue *mua-3(uy19)* lethality at the restrictive temperature, 25°C. Percentage of deaths associated with SODD, *mua-3*, and wild type strains grown at 25°C for 48 hours.

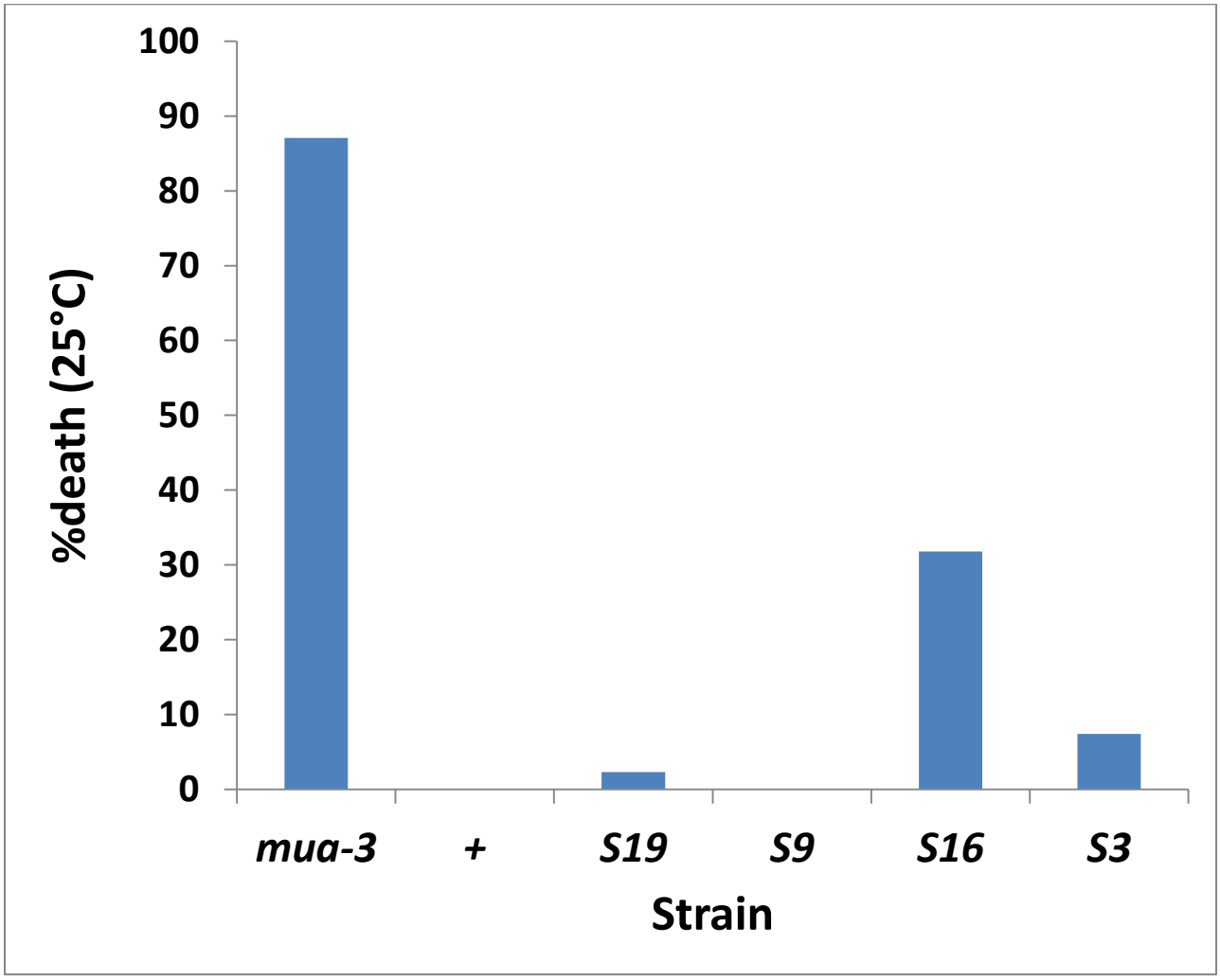
100
90
80
70
60
50
40
30
20
10
0
%death (25°C)
mua-3
+
S19
S9
S16
S3
Strain

2.6 Isolated suppressors rescue *mua-3 (uy19)* lethality phenotype at restrictive temperatures

To confirm the rescue of *mua-3(uy19)* mutated worms by the isolated *mua-3(uy19)* lethality phenotype suppressors, SODDs, *mua-3* mutants and wild type strains were treated at 25°C for 48 hours. The percentage of death for several strains was determined (Figure 11). *mua-3* mutants showed 87% death at 25°C, while wild type and SODD 9 showed 0% death. SODD 19 demonstrated a 2% death, SODD 16 exhibited 32% death, and SODD 3 exhibited 7% death. This confirms that the isolated suppressors of the *mua-3(uy19)* lethality phenotype are capable of inhibiting lethality at restrictive temperatures. The experiment allowed us to move forward in identifying and characterizing the SODDs.

2.7 *dpy-17 mua-3(uy19)* mutants were isolated from separate genetic screens

A series of complementation tests among the isolated suppressors of the *mua-3(uy19)* lethality phenotype, were employed to identify and locate suppressors. Complementation tests among unidentified Dpy suppressor and Sma suppressor phenotypes were performed (Table 4). Unidentified suppressor hermaphrodites were crossed with wild-type males. The F1 progeny males were crossed with an alternate unidentified suppressor. The F1 progeny of this cross were counted and phenotyped as Dpy: wild-type and hermaphrodite: male. If the phenotypic ratio was 1:1, suppressors failed to compliment. Following this, further complementation testing between unknown Dpy suppressors and known *dpy* mutants were performed using the procedure and criteria described above. We determined that 5 suppressors, S9, S19, S11, S18, S23, failed to complement *dpy-17 (e164)(CB164)* (Table 4). The *dpy-17* suppressors of lethality are severely disproportioned and small in size. Suppressors containing a mutated *dpy-17* gene were isolated from two separate forward genetic screens performed on different days. This indicates that not

all isolated suppressors with the mutated *dpy-17* gene were derived from one mother. Through complementation testing we have identified *dpy-17* as a *mua-3* interactor. Further complementation testing may reveal other *mua-3* interactors and enable us to elucidate the mechanisms by which *mua-3* may be involved in TGFβ regulation and MFS disease progression.

Table 4: Summary of Complementation Tests among SODDs (Isolated Suppressors of *mua-3* Lethality)

Strain	Fails To Complement	Complements
dpy-17 (CB164)	S11, S18, S19, S23	
S9		S7, S22
S6		S10
S22	S16	

Figure 12: Percentage of deaths observed for *mua-3(uy19)(YJ35)* worms treated with and without 5ng/ml aztreonum at 25°C (average of 4 worms/treatment). There was no statically significant difference between the aztreonum treated and non-treated conditions. Aztreonum did not sufficiently rescue *mua-3 (uy19)* lethality via connective tissue defect.

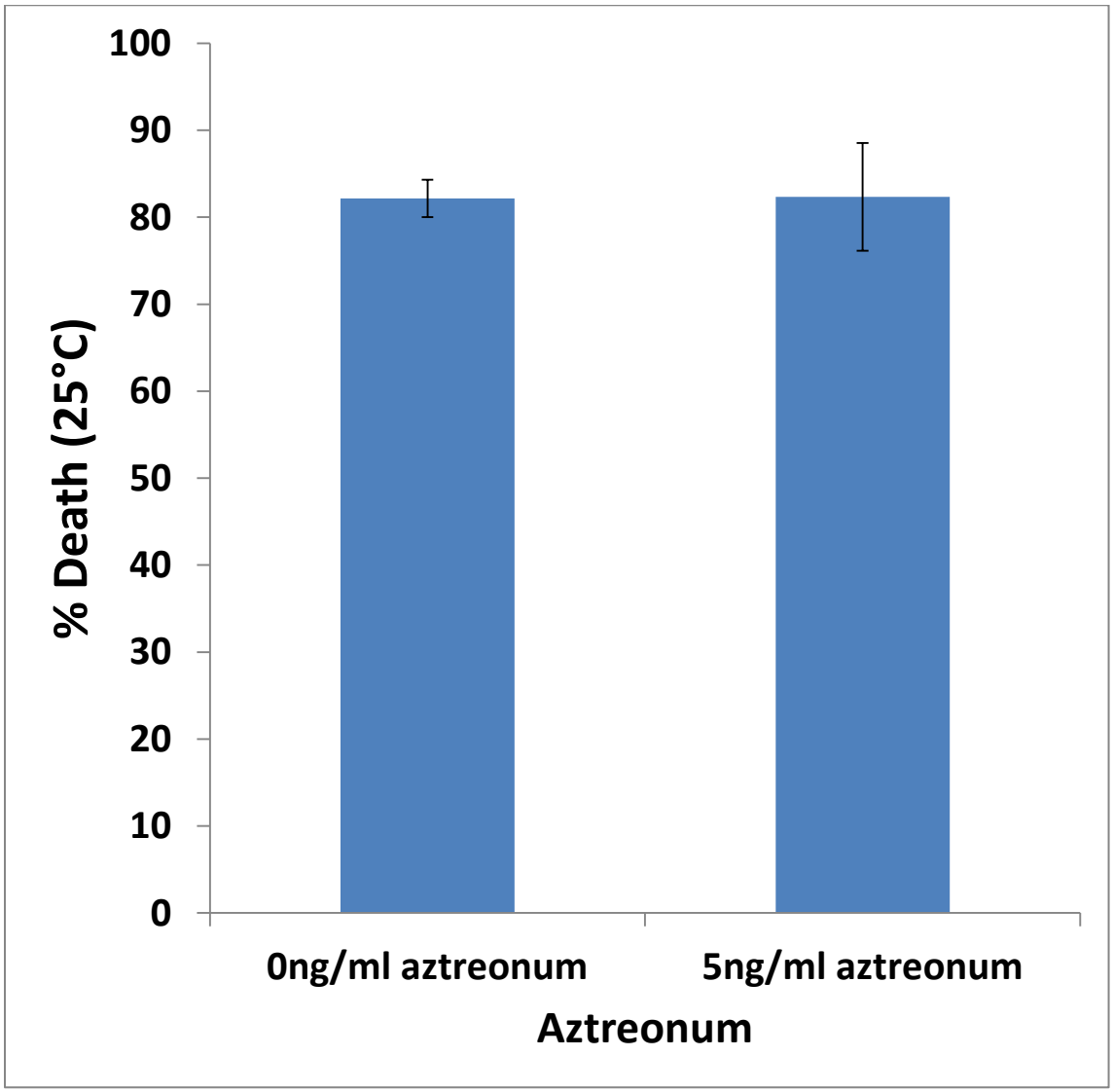
100
90
80
70
60
50
40
30
20
10
0
% Death (25°C)
0ng/ml aztreonum
5ng/ml aztreonum
Aztreonum

2.8 Alterations in nutritional input which decrease metabolism are not sufficient to rescue *mua-3(uy19)* lethality

To determine if *mua-3* mutants are sensitive to fluctuations in metabolic rate mediated by nutritional input, phenotype was assessed at various food quality levels and temperatures (Figure 12). Aztreonum, an inhibitor of bacterial cell wall division, will increase the size of bacteria and thereby decrease food quality. This should reduce metabolic rate and alleviate connective tissue defects leading to lethality. The percentage of death was recorded for both the aztreonum treated and untreated *mua-3(uy19)* mutants at 20°C and 25°C. There was no statistically significant difference in the percentage of death observed at either temperature or aztreonum concentration. This result indicates that 5ng/ml aztreonum is insufficient to rescue *mua-3 (uy19)* lethality and alleviate connective tissue defect. However, this does not exclude the possibility that more severe alterations in nutritional input may alleviate *mua-(uy19)* connective tissue defects and lethality.

3. **DISCUSSION**

3.1 mua-3 connective tissue defects mimic MFS Pathology

The primary aims of this study were to establish a *C.elegans* MFS model by determining how *mua-3*, a fibrillin homolog contributes to the Marfanoid phenotype. Sequence homology and similar phenotypic consequences of mutated genes we and others found indicate the role of fibrillin genes in *C.elegans* and humans is conserved. We have demonstrated that *mua-3* mutant alleles exhibit connective tissue and molting defects, mimicking the MFS phenotype. The lethality *mua-3* occurs during molting and can be attributed to connective tissue defects that lead to internal organ misplacement, connective tissue detachment, or gonadal detachment. These connective tissue defects mimic the symptoms observed in MFS patients.

3.2 The TGFβ pathway regulates body size in *C.elegans* and may interact with *mua-3*

The temperature sensitive nature of the *mua-3 (uy19)* lethality phenotype permitted the use of an unbiased forward genetic screen to isolate suppressors of *mua-3(uy19)* lethality. Several suppressors were isolated, the majority of which had smaller body size and slower growth rate. In *C. elegans*, most genes that regulate body size are components of the TGFβ pathway and all TGFβ mutants exhibit size defects (Fujiwara et al. 2002; Fernando et al. 2011)

Therefore our results provide the first genetic evidence at the organismal level that the fibrillin-1 gene and the TGFβ pathway may interact.

3.3 Latent TGFβ is sequestered by fibrillin-1 and activated by BMP-1, which may have a role in mediating MFS pathology

Upon complementation testing, we identified *dpy-17* mutations as suppressors of the

mua-3(uy19) lethality phenotype from two independent genetic screens. *dpy-17* encodes a cuticle collagen required for posterior outgrowth of *C. elegans*. That we isolated *dpy-17* mutants as a suppressor of mua-3 twice from two independent screens strongly suggests that DPY-17 and MUA-3 interact genetically during L4 molting. Interestingly, gain of function mutations in *dpy-17*, can suppress the *dpy-31*phenotype (Novelli et al. 2004). DPY-31is essential to cuticle formation, embryonic/larval development, is expressed throughout the organism, and is a homolog of Bone Morphogenic Protein-1, a tolloid-like gene responsible for TGFβ activation (Novelli et al. 2004). Therefore, in worms DPY-31 and in humans the BMP-1 metalloprotease may be involved in TGFβ dysregulation, a process that has been previously implicated in MFS disease progression(Ramirez & Dietz 2007).

A disruption in *fbn1* microfibrils can release latent TGFβ(Ramirez & Dietz 2007). Subsequent TGFβ activation results in the production of metalloproteases, and may include BMP-1. BMP-1 may further increase TGFβ activation, by freeing latent complexes from LTBP 1 or degrading LAP(Le Goff & Cormier-Daire 2012). Additionally fibrillin-1 sequesters TGFβ family members including BMPs (Nistala et al. 2010)and it may be that both BMP-1 and latent TGFβ are sequestered by fibrillin-1 rich microfibrils. A disruption in *fbn1* may free latent TGFβ and activators like BMP-1. This may contribute to TGFβ dysregulation and MFS pathology.

3.4 *mua-3 (uy19)* lethality is observed during the L4 stage and may result from mechanical strain, insufficient stage specific cuticle collagen interactions, or insufficient levels of MUA-3, required for molting

Clinical manifestations of MFS appear to be dependent on developmental stage, particularly in adolescence for humans, similar to the L4 stage in worms which precedes reproductive adulthood. There are several plausible reasons for why *mua-3(uy19)* mutants died at

the L4 stage although none have been confirmed experimentally. The MUA-3 protein with 131 amino acid deletion might be able to function until L4 molting but might not be sufficient for L4 molting. The mechanical strain during L4 molt could be more stressful than other molts and result in the lethality phenotype in this particular mutant. An alternative to this hypothesis is that the deleted region of MUA-3 in this mutation contains a domain required for an interaction with an L4 stage specific collagen. This scenario suggests that L4 lethality may be attributed to the specific 131 amino acid in frame deletion mutation of *mua-3 (uy19)*. If *mua-3* interacts with multiple cuticle collagens, another deletion may result in lethality at a different stage.

3.5 Restrictive Temperatures may disrupt protein folding and increase metabolic rate, potentially exacerbating MFS phenotype

Currently MFS is treated with β-adrenergic blockers to lower heart rate, slow aortic growth, and metabolic rate. However, this only ameliorates the deleterious symptoms of progressive aortic root enlargement and aortic dissection(Ramirez & Dietz 2007). As temperature increases, metabolic rate and other processes accelerate. If metabolic rate has any role in regulating disease progression we would expect that an increase in temperature and metabolic rate would exacerbate the MFS-like phenotype whereas a decrease in metabolic rate should alleviate the phenotype. Temperature variation experiments are consistent with the possibility that lethality and sterility phenotypes are exacerbated by higher metabolic rate and alleviated by lower metabolic rate.

Additionally higher temperatures may disrupt proper protein folding. At lower temperatures the protein produced by *mua-3* may be more stable or capable of folding properly. Alternatively the worms may have a protein which is 50% functional at both high and low

temperatures. At low temperatures 50% functionality may be sufficient for survival while at high temperatures 50% functionality of the protein is insufficient. Insufficient levels of functional protein may result in the loss of connective tissue integrity in a temperature dependent manner.

4. Conclusions

Using *C.elegans* as a model for studying MFS, we characterized the temperature sensitive phenotype of *mua-3* and used this characterization to identify genetic interactors of MUA-3. One interactor, DPY-17, is known to genetically interact with DPY-31, a BMP-1 homolog(Novelli et al. 2004). Together, our results suggest that fibrillin-1, TGF-β, and metalloproteases may act in-concert to modulate TGFβ availability and connective tissue integrity in *C. elegans*. These results also show the molecular conservation among known genetic causes for Marfan or Marfan-related syndromes. Furthermore, this suggests that the molting process in *C. elegans* can be used to study Marfan pathology.

4.1 Future Directions

In the future whole genome sequencing can be used to confirm suppressor mutations and further characterize mutations in all isolated suppressors. An *eat-2* loss of function mutation may be introduced into *mua-3* mutants to test whether lowering metabolic rate by reducing food intake alleviates the MFS phenotype and decreases the severity of the connective tissue defect. Additionally, RNAi can be used to inhibit the expression of molecules involved in the TGFβ pathway within *mua-3(uy19)* mutated worms. This technique can be employed to determine the molecular mechanisms by which the severity of connective tissue defect and MFS pathology is enhanced.

5. METHODS

5.1 *C. elegans* strains and culture conditions

Worms were routinely grown on NGMSR plates(Avery 1993). All worms were maintained at 20°C on *E. coli* HB101(Sulston JE 1988) except for *mua-3(uy19) (YJ35)* mutant worms which were maintained at 15°C. The wild-type strain was *C. elegans* variant Bristol, strain N2. Mutant strains used include *mua-3(rh195) (*OT136), *mua-3(uy19)(*YJ35), *dbl-1* (*ctIs40*)(BW1940), *lon-1* (*e185)(CB185), dpy-17 (e164)* (CB164) *and lon-2* (*e678*) (CB678). Eggs were isolated via hypochlorite treatment(Sulston JE 1988) then harvested in M9 buffer to obtain a synchronous population.

5.2 Time course Experiments

Synchronized populations of *mua-3* alleles and wild type strains were transferred to *E.coli* HB101 seeded NGM plates at the L1 stage and cultivated at either 20°C or 25°C in triplicate. Synchronized populations of approximately 100 *mua-3* and wild-type L1s were plated onto each plate. At the L4 stage (after 38 hours at 20'C and 30 hours at 25'C), the number of dead worms and total number of worms were counted to determine percent survival of *mua-3* and wild-type strains at each hour from 38, 30 hours.

5.3 Sterility Phenotype Characterization

To determine the number of offspring produced by individual worms of the *mua-3(rh195)* (OT136) mutants and wild type, approximately10 L4s of each strain were transferred singly to *E. coli*-seeded NGM plates and their progeny counted. Each worm was transferred to a new plate every day to avoid being crowded and to visualize all the progeny easily. Progeny were counted three days later.

5.4 Body Length Measurements

Body lengths of the wild type (N2), *mua-3(rh195) (*OT136), *mua-3(uy19)(*YJ35), *dbl-1* (*ctIs40*)(BW1940), *lon-1* (*e185)(CB185), and lon-2* (*e678*) (CB678) were measured.. Worms of each strain were picked at the L4 stage and measured their body lengths at 24, 48, and 72 hours using Differential Interference Contrast (DIC) light microscopy at the settings of 10X objective, III condenser, 0.3 aperture, 100ms exposure and a scale bar of 100 micrometers was used in making the measurement calculations.

Additionally, in order to allow worms to successfully pass the L4 stage, measurements were taken after incubating L4s of wild-type (N2), *mua-3(rh195) (*OT136), *mua-3(uy19)(*YJ35), *dbl-1* (*ctIs40*)(BW1940), *lon-1* (*e185)(CB185), and lon-2* (*e678*) (CB678) at 15°C for 24 hours then transferring the strains to 20°C. Worms were imaged using DIC microscopy as described above.

To determine the size and potentially enhance the long length phenotype, synchronized populations of *mua*-3*(rh195)(OT136)* mutant and wild type were transferred to 25°C . Worms were imaged at approximately 24 and 48 hours after L4 stage using DIC microscopy as described above.

5.5 Nutritional Variation

LB agar was prepared with and without 5 ng/ml concentration of aztreonam, which decreases food quality by inhibiting bacterial cell wall division (ref). Following agar preparation, plates were seeded with *E. coli* HB101 (incubated at 37°C for 12 hours and cooled for 24 hours

prior to use). *mua-3* mothers (n=4) were then moved to aztreonam-treated and untreated plates (in duplicate). Aztreonam-treated and untreated plates were then placed either at 20°C or 25°C. Mothers were aspirated after 5 hours, in order to synchronize the population. Forty-eight hours later, the number of dead worms and total number of worms were counted to determine percent death.

5.6 Determination of Temperature for Suppressor Screen

Using age matched plates, wild type and *mua-3* mutant strains at the L1 stage were transferred to 20°C or 25°C (duplicate). At the L4 stage, the number of dead worms and total number of worms were counted to determine percent survival. This was done to establish an appropriate temperature treatment for use in an F2 suppressor screen of mutagenized *mua-3* worms.

5.7 Suppressor Screen

mua-3(uy19) (YJ35) worms were collected at L4 stage and randomly mutagenized with ethyl methane sulphate (EMS) (Riddle DL, Blumenthal T, Meyer BJ, et al. 1997; Brenner 1974). P_o worms were plated onto *E.coli* HB101 seeded plates and moved to 15°C. F1 progeny were synchronized and remained at 15°C. The homozygous, F2 generation was synchronized and moved to 25°C. Survived worms (suppressors of *mua-3* mutant phenotype, SODD) were isolated.

5.8 Secondary screen

Individual suppressors of the *mua-3* mutant phenotype were isolated and moved to individual plates at the restrictive temperature, 25°C. Sterile (worms that produced no progeny)

and escaper worms (worms that produced over 90% of non-viable progeny) were removed. F2s, approximately 20 were isolated and maintained at 25°C.

5.9 Complementation Test

Complementation tests among unidentified Dpy phenotypes and Sma phenotypes were performed. Unidentified suppressor hermaphrodites were crossed with wild-type males. The F1 progeny males were crossed with an alternate unidentified suppressor. The F1 progeny of this cross were counted to calculate the percentage of Dpy. The percentage of males in the population was also counted to determine whether Dpy progeny is from cross or self-fertilization. If 50% of the progeny is Dpy, suppressors failed to complement each other.

5.10 Confirmation of Suppressors

To determine if the suppressors of *mua-3* lethality (Suppressor Of Drop Dead, SODD) isolated from the screen are capable of rescuing the *mua-3 (uy19)* mutant at 25°C, *mua-3*, wild type, and SODD strains were synchronized, individually plated, and moved to 25°C. The number of dead worms and total number of worms were counted to determine percent survival of each strain.

5.11 Analysis

Student t-tests were performed to determine statistical significance.

Appendix A

Quiescence is marked by inactivity, reflecting the nutritional state of full feeding. The behavior is mediated by TGFβ, insulin, and cGMP (cyclic guanosine monophosphate) pathways (You et al. 2008). In this study, we aimed to determine whether increasing cGMP levels through administration of sildenafil citrate increases satiety quiescence. Sildenafil citrate, a phosphodiesterase inhibitor, prevents the breakdown of cGMP and therefore increases cGMP signals. Sildenafil citrate has been shown to provide protective effects against weight gain on high fat diets both in humans and mice. We found that quiescence following sildenafil citrate treatment at certain concentrations was enhanced. Statistical significance was observed in only one set of data and not reproduced in subsequent experiments. However inconclusive our results are, we could observe the trend that sildenafil citrate could potentially alter satiety quiescence, therefore could be further used as a pharmacological tool to study how enhanced cGMP signaling can affect satiety quiescence in *C. elegans*. Addressing this will help to study whether a commercially available drug such as sildenafil citrate can be used to treat obesity to suppress appetite control.

A. Introduction

A.1 Obesity

Obesity is the leading cause of the two deadliest diseases in the US, cardiovascular disease and type 2 diabetes. Yet, the underlying molecular mechanisms that contribute to obesity are poorly understood. Nonetheless, Valentino *et.al.*(Valentino MA, Lin JE, Snook AE, Li P, Kim GW, Marszalowicz G, Magee MS, Hyslop T, Schulz S 2011) recently uncovered that a cGMP pathway is stimulated upon feeding to suppress appetite. Similarly, recent reports demonstrate that sildenafil citrate, a medicine that inhibits degradation of cGMP to treat erectile dysfunction, has protective effects against weight gain on a high-fat diet both in humans and mice. Together, these findings highlight an essential role for cGMP signaling (Valentino MA, Lin JE, Snook AE, Li P, Kim GW, Marszalowicz G, Magee MS, Hyslop T, Schulz S 2011)in appetite and metabolism and further suggest that well-established pharmacological inhibitors may be effective treatments for obesity.

A.2 Satiety Quiescence

Quiescence results from satiety and is indicated by the behavioral sequence of satiety, in which animals stop feeding and moving and rest(Sengenès et al. 2000). The main regulators of quiescence are TGFβ, insulin, and cGMP. The cGMP pathway is particularly important because a mutation in cGMP-dependent kinase (PKG) completely abolishes satiety quiescence(You et al. 2008). However, in *C.elegans*, the cellular and molecular mechanisms by which cGMP regulates satiety quiescence is unclear(You et al. 2008).

cGMP signaling pathways regulate phototransduction, vasodilation, glucagon secretion, mitochondrial biogenesis, brown adipocyte tissue formation, and cellular metabolism(Mitschke

et al. 2013). cGMP signals also participate in sleep and feeding in invertebrates(Fujiwara et al. 2002; You et al. 2008). Additionally cGMP contributes to adipocytokine secretion, adipocyte size, and maintenance of healthy white adipose tissue (WAT)(Mitschke et al. 2013).

A.3 cGMP

cGMP mediates effects through cyclic nucleotide gated ion channels, cGMP regulated phosphodiesterases, and cGMP-dependent protein kinase G (PKG)(Francis et al. 2010). In the *C.elegans daf*-11mutant, the loss of function of a membrane bound guanylyl cyclase, a producer of cGMP(Jennissen et al. 2012), will result in shorter quiescence than wild type(Mitschke et al. 2013; Birnby et al. 2000). PKG is activated by cGMP (Jennissen et al. 2012) and responsible for olfactory adaptation, locomotion behavior, regulating body size(Fujiwara et al. 2002; Hirose 2003; L'Etoile et al. 2002), lipolysis (via hormone sensitive lipase)(Sengenès et al. 2000), and has a role in food seeking behavior(Ben-Shahar et al. 2002) (Figure 13)(You et al. 2008). The gain of function mutation of PKG (EGL-4) is smaller than wild type and exhibits quiescence(Raizen et al. 1995) while the loss of function is larger than wild type and roams more often (Raizen et al. 1995). Data from these experiments show decreases in cGMP levels or cGMP signaling results in less quiescence and that cGMP is crucial to normal satiety quiescence.

Figure 13: Pathway for induction of satiety quiescence mediated by cGMP, TGFβ, and insulin. (You et al. 2008)

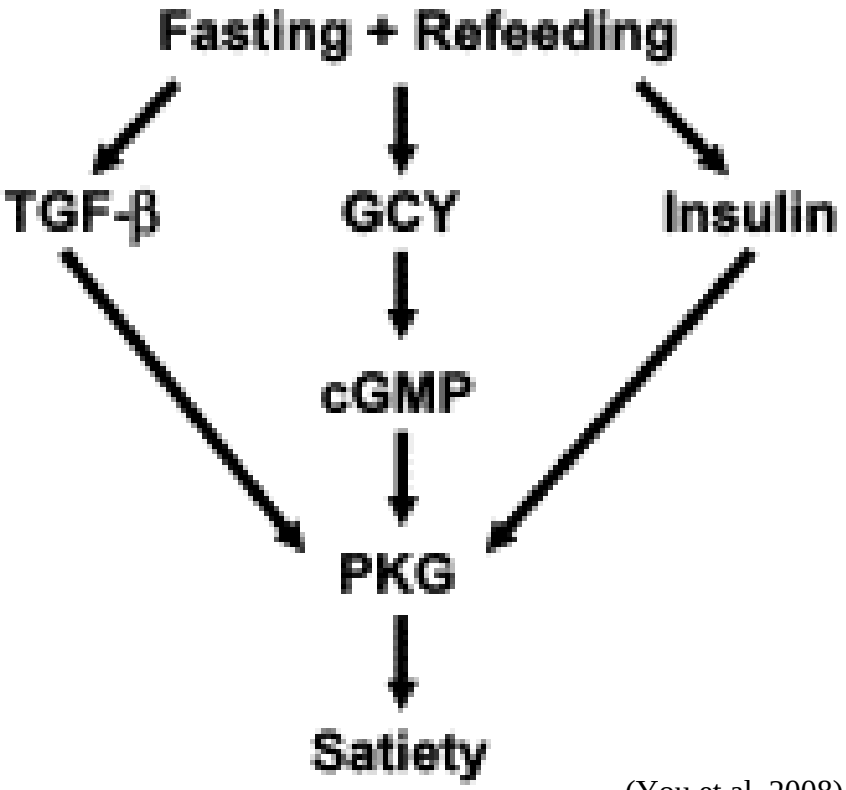

(You et al. 2008)

A.4 cGMP Involvement in Obesity Prevention and Insulin Sensitization

White adipocytes contain the largest energy reserves and possess endocrine functions(Mitschke et al. 2013). cGMP induces browning of WAT through the cGMP/PKG1 pathway(Mitschke et al. 2013). PKG-1 regulates cell size, adipokine secretion, and is required for the differentiation of white adipocytes into brown adipocytes(Haas et al. 2009). Brown adipocytes metabolize fatty acids (Antin et al. 1975); this process depends on the number of mitochondria and amount of uncoupling protein-1 expressed(Cannon & Nedergaard 2004). By uncoupling mitochondorial oxidative phosphorylation, UCP-1 dissipates the energy from fatty acids as heat (Okamatsu-Ogura et al. 2013) (Cannon & Nedergaard 2004) and is only seen in brown adipose tissue (BAT)(Antin et al. 1975). Following treatment with cGMP, white adipocytes undergo phenotypic trans-differentiation to become beige adipocytes (Mitschke et al. 2013). Beige adipocytes express PGC-1 alpha, express high levels of mitochondria and UPC-1 (due to cGMP/PKG1 signaling)(Nedergaard & Cannon 2010; Lowell & Spiegelman 2000) and mediate norepinephrine thermogenesis. Although developmentally distinct, brown and beige adipocytes function physiologically to generate heat via UCP-1, thus protect against hypothermia and obesity(Wu et al. 2012; Okamatsu-Ogura et al. 2013; Mitschke et al. 2013) . cGMP's role in brown adipocyte differentiation in white adipose tissue implies that cGMP may be involved in obesity prevention (Mitschke et al. 2013).

Adipokines are involved in glucose metabolism and in, inflammation, and contribute to a higher risk of diseases associated with obesity (Mitschke et al. 2013). Following cGMP treatment (PKG1 activation), adiponectin levels increased whereas proinflammatory cytokine levels were decreased(Mitschke et al. 2013). Proinflammatory cytokines are typically upregulated in obese individuals and add to macrophage infiltration into adipose tissue(Mitschke

et al. 2013) whereas low levels of adiponectin are associated with insulin resistance and obesity(Arita et al. 2012). cGMP's role in proinflammatory adipokine reduction and adiponectin enhancement suggests cGMP may be decrease insulin resistance (Mitschke et al. 2013).

A.5 Sildenafil Citrate

Sildenafil citrate has been shown to endow protective effects in weight gain from high fat diets. This PDE inhibitor is selective for PDE 5 and will increase cGMP levels by preventing hydrolysis of cGMP(Valtcheva et al. 2009; Burkhardt et al. 2000). Chronic cGMP hydrolysis inhibition increases insulin action while short term cGMP hydrolysis inhibition increases browning of white adipocyte tissue. Short term sildenafil citrate treatment will increase UPC-1 expression and PGC-1 alpha expression in WAT (Mitschke et al. 2013). This is indicative of transdifferentiation into brown adipocytes. Increased browning of WAT, referred to as beige adipose tissue, and increased brown adipocyte levels lead to greater energy expenditure and weight loss(Mitschke et al. 2013; Ayala et al. 2007).

Using the phosphodiesterase inhibitor, sildenafil citrate, we aimed to test whether increased cGMP levels would enhance quiescence. We treated worms with various concentrations of sildenafil citrate, monitored locomotion using the YouWorm Tracking system, a custom written program in Matlab and analyzed the locomotion data with a custom written program in Mathematica. Quiescence was indicated by a lower average speed and higher time at low speed for worm locomotion. We found that sildenafil citrate treatment consistently enhanced quiescence at certain concentrations however the result did not reach statistical significance.

The trend that sildenafil citrate potentially alters satiety quiescence, suggests that it is valuable as a tool for studying how enhanced cGMP signaling can affect satiety quiescence in *C. elegans*. Addressing this will help ascertain whether a commercially available drug such as sildenafil citrate can be used to treat obesity by suppressing appetite.

B. RESULTS

B.1 Sildenafil Citrate Treated Worms had a Lower Average Speed and Spent more Time at Low Speed than Control Worms

The trend among the increasing concentrations of sildenafil citrate appeared to show enhanced quiescence at lower concentrations and then a plateau at concentrations above 20µM sildenafil citrate treatment. The amount of time spent at low speed was enhanced for worms treated with 10 µM or 20 µM sildenafil citrate in comparison to the DMSO control (Figure 14 B). However, there appeared to be a plateau in the amount of time spent at low speed for concentrations above 20µM sildenafil citrate. Control (water and DMSO) treated worms had a higher average speed compared to the 10 µM treated worms, and 20 µM treated worms had a lower average speed than 10µM treated worms (Figure 14 A). Treatment with 20µM sildenafil citrate showed enhanced quiescence and decreased roaming. Concentrations above 20 µM showed an increase in average speed when compared to the 20 µM treated worms. Hidden Markov Model analysis permitted the tracking of individual worm satiety state via locomotion data (Gallagher 2013). This data shows the total time spent in dwelling (feeding while motionless), roaming (actively seeking food), and quiescence states. The results indicate that at the 20 µM concentration of sildenafil citrate, quiescence is enhanced compared to both controls (Figure 14 C). (Data obtained from experiments with various sildenafil citrate concentrations and concurrent DMSO controls demonstrates the same trend described above.) We found that enhanced quiescence following sildenafil citrate treatment at certain concentrations was enhanced. Statistical significance was observed in only one set of data and not reproduced in subsequent experiments. The average of three experiments performed, on the same day showed a statistically significant difference between the DMSO control and sildenafil citrate treated worms

(20 µM and 30µM). Using the same experimental procedure, we provide three different forms of analysis which all indicate the 20µM concentration of sildenafil citrate enhances quiescence. These experiments allowed us to determine amount of quiescence at each treatment by several parameters.

Figure 14A: Representative graph of the average speed of worms treated with water only, DMSO only, or various concentrations of sildenafil citrate for 24 hours. (3 worms/ treatment concentration; n=3) B: Representative graph of time at low speed of worms treated with water, DMSO only, or various concentrations of sildenafil citrate for 24 hours. (3 worms/ treatment concentration; n=3) Worm locomotion data for Figure 14A and 14B was monitored via YouWorm Tracking system, a custom written program in Matlab, for 1800 frames (985ms/1800000ms) and analyzed with a custom written program in Mathematica. C: HMM analysis of several worms drug treated with various concentrations of sildenafil citrate. Controls were vehicle treated DMSO (1.6%) or non-treated with water (DMSO_C). Red; Roaming; Blue; quiescence; Green; dwelling. Numbers listed on the bottom of the Figure 14 C indicate the percentage of time spent in each state. Parenthetical numbers listed to the side indicate the number of worms for each treatment. Worm locomotion data was monitored via YouWorm Tracking system for 1800 frames (985ms/1800000ms) and analyzed using a custom written program in Matlab.

A

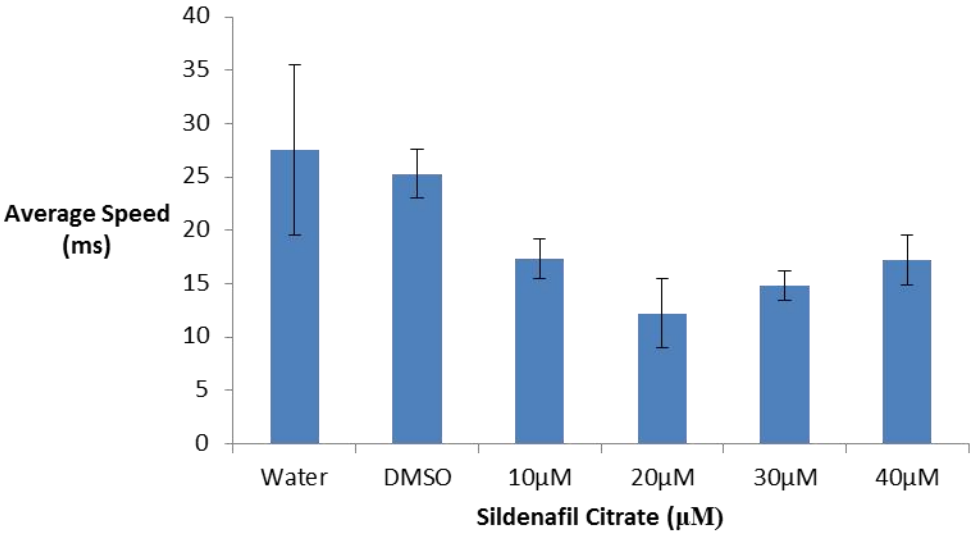
Average Speed (ms)
40
35
30
25
20
15
10
5
0
Water
DMSO
10µM
20µM
30µM
40µM
Sildenafil Citrate (µM)

B

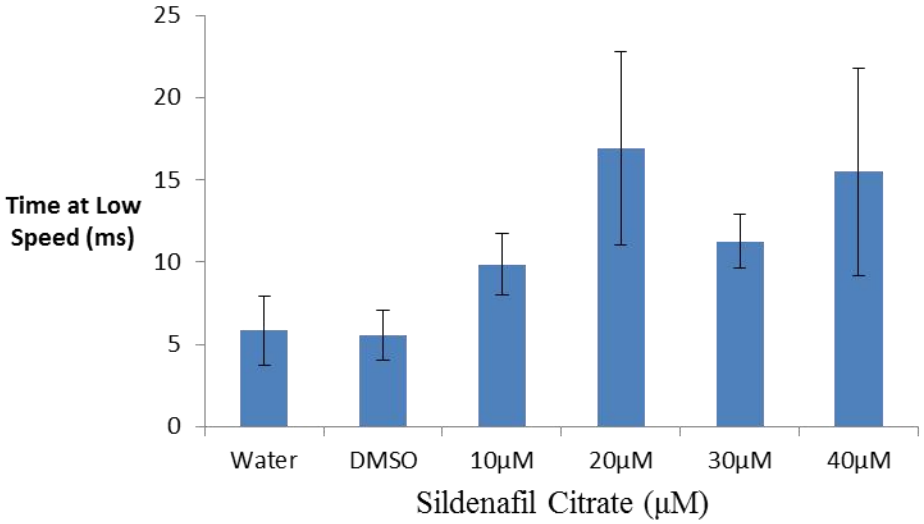
Time at Low Speed (ms)
25
20
15
10
5
0
Water
DMSO
10µM
20µM
30µM
40µM
Sildenafil Citrate (µM)

C

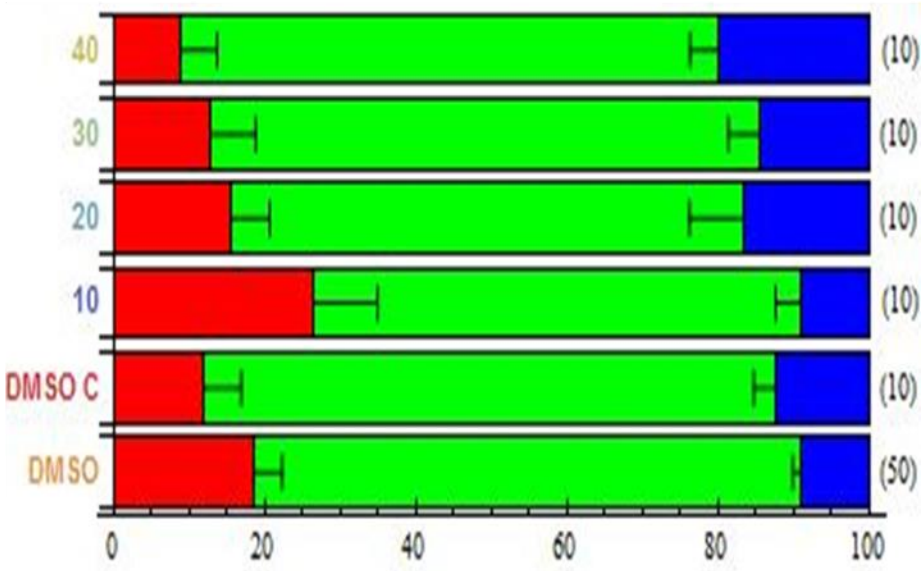
40
30
20
10
DMSO C
DMSO
(10)
(10)
(10)
(10)
(10)
(50)
0
20
40
60
80
100

C. DISCUSSION

C.1 Sildenafil Citrate May Enhance Satiety Quiescence

The primary aim of this study was to determine whether sildenafil citrate can enhance quiescence and address whether the drug is viable for use in determining the mechanism by which cGMP enhances quiescence. The PDE inhibitor sildenafil citrate prevents the hydrolysis of cGMP, thereby increasing cGMP levels. We hypothesized that an increase in cGMP signal duration could mediate downstream effects that result in enhanced quiescence. Enhanced amount of time at low speed and reduced average speed were the parameters used to indicate worm quiescence. We observed an enhanced time at low speed and reduced average speed in sildenafil citrate treated worms in comparison with the DMSO control. Additionally, HMM analysis indicated enhanced quiescence in worms treated with 20 µM sildenafil citrate.

A statistically significant difference between the DMSO control and sildenafil citrate treated worms (20µM and 30 µM) was observed in only one set of data and not reproduced in subsequent experiments. Overall, the trend observed was that of enhanced quiescence with increasing concentrations of sildenafil citrate until reaching 30µM sildenafil citrate. The enhancement of satiety quiescence plateaued at concentrations above 20 µM sildenafil citrate. Here, we propose a potential mechanism for the observed trend in satiety quiescence mediated by sildenafil citrate. Sildenafil citrate in the *C. elegans* intestine can act on PDE and multi drug resistance (MRP) proteins, which transport molecules through the cell membrane. It has been previously determined that satiety quiescence in a *C. elegans mrp-6* knockout mutant is reduced (Gallagher 2013). Sildenafil citrate acts on PDE in the neuron only and PDE molecules may

become saturated in the neuron. At high concentrations MRP may be blocked by sildenafil citrate and cGMP cannot leave the gut and there is no more increase in quiescence observed.

D. METHODS

D.1 *C. elegans* Strains and Culture Conditions

Worms were routinely grown on NGMSR plates(Avery 1993). All worms were maintained at 20°C on *E. coli* HB101(Sulston JE 1988). The wild-type strain was *C. elegans* variant Bristol, strain N2. During experimental treatment with sildenafil citrate worms were fed with HB101*E.coli*, cultured overnight and cooled for 24 hours prior to feeding worms.

D.2 Sildenafil Citrate Treatment Preparation

Sildenafil citrate was diluted in DMSO to obtain stock solutions of 20 mM and 40 mM. Sildenafil citrate diluted with M9 (150 µL of solution) was pipetted onto an NGM plate and allowed to dry for one hour. Following the same procedure, a DMSO and M9 solution were prepared to use as control treatments. LB (5 ml) was inoculated with *E.coli* HB101 and allowed to incubate on a shaker at 37°C at 250 rpm for 24 hours, then cooled to room temperature for 24 hours, before centrifugation at 4000 rpm for three minutes and removal of most of the supernatant. The *E. coli* HB101 remaining was pipetted in order to liquefy the bacteria and diluted with 2 1:1 serial dilutions in M9 and 10 µL was administered onto each plate and permitted to dry for ten minutes.

D.3 Measuring Locomotive Activity and Analysis

Approximately 5 L4 wild type worms were moved to the sildenafil citrate containing plates with concentrations of 10µM, 20µM, 30µM, or 40µM; 5 L4 worms were placed onto the control plates containing 1.6 % DMSO; 5 L4 worms were placed onto the control plates containing water; the worms were treated with sildenafil citrate, 1.6% DMSO as a control, or with water as

a control, at 20°C for 24 hours. Non-treated (water), vehicle treated (1.6% DMSO), and drug treated sildenafil citrate (10µM, 20µM, 30µM, or 40µM) plates were prepared with freshly made solutions. The single vehicle treated DMSO control was used in order to control for the potential effect of various volumes of DMSO used in concurrent trial controls. The plates were dried for one hour, then 4 µL of freshly diluted *E. coli* HB101 (food for worms) was added to each plate After 10 minutes when the plates were dried, a single worm from each treatment plate was transferred to an individual treatment plate corresponding to the initial treatment. The worms were allowed to habituate for 30 minutes prior to being monitored with cameras for 1800 frames, an image was captured every 985ms for 1800000ms. The data was collected with the YouWorm Tracking system, a custom written program in Matlab, the locomotion data was analyzed with a custom written program in Mathematica as well as HMM analysis to determine quiescence. Student t-tests and ANOVA were performed to determine statistical significance.

References

Altschul SF1, Gish W, Miller W, Myers EW, L.D., 1990. Basic local alignment search tool. *J Mol Biol.*, 215(3), pp.403–10.

Altun, Z. F. and Hall, D.H., 2005. Handbook of C. elegans Anatomy. In Wormatlas. Available at: (http://www.wormatlas.org/ver1/handbook/anatomyintro/anatomyintro.htm).

Antin, J. et al., 1975. Cholecystokinin elicits the complete behavioral sequence of satiety in rats. *Journal of comparative and physiological psychology*, 89(7), pp.784–90. Available at: http://www.ncbi.nlm.nih.gov/pubmed/1176672.

Arita, Y. et al., 2012. Paradoxical decrease of an adipose-specific protein, adiponectin, in obesity. 1999. *Biochemical and biophysical research communications*, 425(3), pp.560–4. Available at: http://www.ncbi.nlm.nih.gov/pubmed/22925674.

Avery, 2007. C. elegans as a Model System. Available at: http://avery.rutgers.edu/WSSP/StudentScholars/project/introduction/worms.html.

Avery, L., 1993. The genetics of feeding in Caenorhabditis elegans. *Genetics*, 4(133), pp.897–917.

Avery, L. & You, Y., 2012. C. elegans feeding. , p.http://www.wormbook.org/chapters/www_feeding/feedi.

Ayala, J.E. et al., 2007. Mice. , 56(April), pp.1025–1033.

De Backer, J., Loeys, B. & De Paepe, a., 2009. Marfan and Marfan-like syndromes. *Artery Research*, 3(1), pp.9–16. Available at: http://linkinghub.elsevier.com/retrieve/pii/S1872931209000040 [Accessed April 28, 2014].

Ben-Shahar, Y. et al., 2002. Influence of gene action across different time scales on behavior. *Science (New York, N.Y.)*, 296(5568), pp.741–4. Available at: http://www.ncbi.nlm.nih.gov/pubmed/11976457 [Accessed April 28, 2014].

Bercher, M., 2001. mua-3, a gene required for mechanical tissue integrity in Caenorhabditis elegans, encodes a novel transmembrane protein of epithelial attachment complexes. *The Journal of Cell Biology*, 154(2), pp.415–426. Available at: http://www.jcb.org/cgi/doi/10.1083/jcb.200103035 [Accessed April 28, 2014].

Birnby, D.A. et al., 2000. Common Set of Chemosensory Behaviors in Caenorhabditis elegans. , 90.

Booms, P. et al., 2005. RGD-containing fibrillin-1 fragments upregulate matrix metalloproteinase expression in cell culture: a potential factor in the pathogenesis of the

Marfan syndrome. *Human genetics*, 116(1-2), pp.51–61. Available at: http://www.ncbi.nlm.nih.gov/pubmed/15517394 [Accessed April 29, 2014].

Brenner, S., 1974. Caenorhabdztzs elegans. , pp.71–94.

Buechner, M., 2002. Tubes and the single C. elegans excretory cell. *Trends in cell biology*, 12(10), pp.479–84. Available at: http://www.ncbi.nlm.nih.gov/pubmed/12441252.

Burkhardt, M. et al., 2000. KT5823 inhibits cGMP-dependent protein kinase activity in vitro but not in intact human platelets and rat mesangial cells. *The Journal of biological chemistry*, 275(43), pp.33536–41. Available at: http://www.ncbi.nlm.nih.gov/pubmed/10922374 [Accessed April 28, 2014].

Cannon, B. & Nedergaard, J., 2004. Brown adipose tissue: function and physiological significance. *Physiological reviews*, 84(1), pp.277–359. Available at: http://www.ncbi.nlm.nih.gov/pubmed/14715917.

Culetto, E. & Sattelle, D.B., 2000. A role for Caenorhabditis elegans in understanding the function and interactions of human disease genes. *Human molecular genetics*, 9(6), pp.869–77. Available at: http://www.ncbi.nlm.nih.gov/pubmed/10767309.

Fernando, T. et al., 2011. C. elegans ADAMTS ADT-2 regulates body size by modulating TGFβ signaling and cuticle collagen organization. *Developmental biology*, 352(1), pp.92–103. Available at: http://www.pubmedcentral.nih.gov/articlerender.fcgi?artid=3049821&tool=pmcentrez&rendertype=abstract [Accessed April 28, 2014].

Francis, S.H. et al., 2010. cGMP-dependent protein kinases and cGMP phosphodiesterases in nitric oxide and cGMP action. *Pharmacological reviews*, 62(3), pp.525–63. Available at: http://www.pubmedcentral.nih.gov/articlerender.fcgi?artid=2964902&tool=pmcentrez&rendertype=abstract.

Frand, A.R., Russel, S. & Ruvkun, G., 2005. Functional genomic analysis of C. elegans molting. *PLoS biology*, 3(10), p.e312. Available at: http://www.pubmedcentral.nih.gov/articlerender.fcgi?artid=1233573&tool=pmcentrez&rendertype=abstract [Accessed April 28, 2014].

Fujiwara, M., Sengupta, P. & McIntire, S.L., 2002. Regulation of body size and behavioral state of C. elegans by sensory perception and the EGL-4 cGMP-dependent protein kinase. *Neuron*, 36(6), pp.1091–102. Available at: http://www.ncbi.nlm.nih.gov/pubmed/12495624.

Gallagher, T., 2013. © Thomas L. Gallagher, 2013 All Rights Reserved.

Gao, L.G. et al., 2010. Recent molecular biological progress in Marfan syndrome and Marfan-associated disorders. *Ageing Research Reviews*, 9(3), pp.363–368. Available at: http://www.ncbi.nlm.nih.gov/pubmed/19772952 [Accessed April 28, 2014].

Le Goff, C. & Cormier-Daire, V., 2012. From tall to short: the role of TGFβ signaling in growth and its disorders. *American journal of medical genetics. Part C, Seminars in medical genetics*, 160C(3), pp.145–53. Available at: http://www.ncbi.nlm.nih.gov/pubmed/22791552 [Accessed April 28, 2014].

Guo, G. et al., 2006. Induction of macrophage chemotaxis by aortic extracts of the mgR Marfan mouse model and a GxxPG-containing fibrillin-1 fragment. *Circulation*, 114(17), pp.1855–62. Available at: http://www.ncbi.nlm.nih.gov/pubmed/17030689 [Accessed April 29, 2014].

Haas, B. et al., 2009. Protein kinase G controls brown fat cell differentiation and mitochondrial biogenesis. *Science signaling*, 2(99), p.ra78. Available at: http://www.ncbi.nlm.nih.gov/pubmed/19952371 [Accessed April 28, 2014].

Handford, 2012. No Title.

Hirose, T., 2003. Cyclic GMP-dependent protein kinase EGL-4 controls body size and lifespan in C. elegans. *Development*, 130(6), pp.1089–1099. Available at: http://dev.biologists.org/cgi/doi/10.1242/dev.00330 [Accessed April 28, 2014].

Horiguchi, M., Ota, M. & Rifkin, D.B., 2012. Matrix control of transforming growth factor-β function. *Journal of biochemistry*, 152(4), pp.321–9. Available at: http://www.pubmedcentral.nih.gov/articlerender.fcgi?artid=3529568&tool=pmcentrez&rendertype=abstract [Accessed April 28, 2014].

Jennissen, K. et al., 2012. A VASP-Rac-soluble guanylyl cyclase pathway controls cGMP production in adipocytes. *Science signaling*, 5(239), p.ra62. Available at: http://www.ncbi.nlm.nih.gov/pubmed/22932701 [Accessed April 28, 2014].

Joyce, T.D., 2011. MFS Individual. Available at: https://www.broadinstitute.org/blog/marfan-syndrome-gene-drug.

L'Etoile, N.D. et al., 2002. The cyclic GMP-dependent protein kinase EGL-4 regulates olfactory adaptation in C. elegans. *Neuron*, 36(6), pp.1079–89. Available at: http://www.ncbi.nlm.nih.gov/pubmed/12495623.

Lee, I. et al., 2012. Metabolic rate regulates L1 longevity in C. elegans. *PloS one*, 7(9), p.e44720. Available at: http://www.pubmedcentral.nih.gov/articlerender.fcgi?artid=3435313&tool=pmcentrez&rendertype=abstract [Accessed April 28, 2014].

Van der Linden, A.M. et al., 2008. The EGL-4 PKG acts with KIN-29 salt-inducible kinase and protein kinase A to regulate chemoreceptor gene expression and sensory behaviors in Caenorhabditis elegans. *Genetics*, 180(3), pp.1475–91. Available at: http://www.pubmedcentral.nih.gov/articlerender.fcgi?artid=2581950&tool=pmcentrez&rendertype=abstract [Accessed April 28, 2014].

Lowell, B.B. & Spiegelman, B.M., 2000. Towards a molecular understanding of adaptive thermogenesis. *Nature*, 404(6778), pp.652–60. Available at: http://www.ncbi.nlm.nih.gov/pubmed/10766252.

Massagué, J., Blain, S.W. & Lo, R.S., 2000. TGFbeta signaling in growth control, cancer, and heritable disorders. *Cell*, 103(2), pp.295–309. Available at: http://www.ncbi.nlm.nih.gov/pubmed/11057902.

Mitschke, M.M. et al., 2013. Increased cGMP promotes healthy expansion and browning of white adipose tissue. *FASEB journal : official publication of the Federation of American Societies for Experimental Biology*, 27(4), pp.1621–30. Available at: http://www.ncbi.nlm.nih.gov/pubmed/23303211 [Accessed April 28, 2014].

Nedergaard, J. & Cannon, B., 2010. The changed metabolic world with human brown adipose tissue: therapeutic visions. *Cell metabolism*, 11(4), pp.268–72. Available at: http://www.ncbi.nlm.nih.gov/pubmed/20374959 [Accessed April 28, 2014].

Nistala, H. et al., 2010. Fibrillin-1 and -2 differentially modulate endogenous TGF-β and BMP bioavailability during bone formation. *The Journal of cell biology*, 190(6), pp.1107–1121. Available at: http://www.pubmedcentral.nih.gov/articlerender.fcgi?artid=3101602&tool=pmcentrez&rendertype=abstract [Accessed April 28, 2014].

Novelli, J., Ahmed, S. & Hodgkin, J., 2004. Gene interactions in Caenorhabditis elegans define DPY-31 as a candidate procollagen C-proteinase and SQT-3/ROL-4 as its predicted major target. *Genetics*, 168(3), pp.1259–73. Available at: http://www.pubmedcentral.nih.gov/articlerender.fcgi?artid=1448789&tool=pmcentrez&rendertype=abstract [Accessed April 28, 2014].

Okamatsu-Ogura, Y. et al., 2013. Thermogenic ability of uncoupling protein 1 in beige adipocytes in mice. *PloS one*, 8(12), p.e84229. Available at: http://www.pubmedcentral.nih.gov/articlerender.fcgi?artid=3875535&tool=pmcentrez&rendertype=abstract [Accessed May 2, 2014].

Raizen, D.M., Lee, R.Y.N. & Avery, L., 1995. Interacting Genes Required for Pharyngeal Excitation by Motor Neuron MC i n.

Ramirez, F. & Dietz, H.C., 2007. Marfan syndrome: from molecular pathogenesis to clinical treatment. *Curr Opin Genet Dev*, 17(3), pp.252–258. Available at: http://www.ncbi.nlm.nih.gov/pubmed/17467262 [Accessed April 28, 2014].

Riddle DL, Blumenthal T, Meyer BJ, et al., 1997. C. elegans II. 2nd edition. Available at: http://www.ncbi.nlm.nih.gov/books/NBK20086/.

Sengenès, C. et al., 2000. Natriuretic peptides: a new lipolytic pathway in human adipocytes. *FASEB journal : official publication of the Federation of American Societies for*

Experimental Biology, 14(10), pp.1345–51. Available at: http://www.ncbi.nlm.nih.gov/pubmed/10877827.

Sengle, G. et al., 2008. Targeting of bone morphogenetic protein growth factor complexes to fibrillin. *The Journal of biological chemistry*, 283(20), pp.13874–13888. Available at: http://www.pubmedcentral.nih.gov/articlerender.fcgi?artid=2376219&tool=pmcentrez&rendertype=abstract [Accessed April 28, 2014].

Sulston JE, H.J., 1988. In: The Nematode Caenorhabditis elegans. *Methods*, pp.587–606.

Valentino MA, Lin JE, Snook AE, Li P, Kim GW, Marszalowicz G, Magee MS, Hyslop T, Schulz S, W.S., 2011. A uroguanylin-GUCY2C endocrine axis regulates feeding in mice. *J Clin Invest.*, 9(121), pp.3578–88.

Valtcheva, N. et al., 2009. The commonly used cGMP-dependent protein kinase type I (cGKI) inhibitor Rp-8-Br-PET-cGMPS can activate cGKI in vitro and in intact cells. *The Journal of biological chemistry*, 284(1), pp.556–62. Available at: http://www.ncbi.nlm.nih.gov/pubmed/19008225 [Accessed April 28, 2014].

Wu, J. et al., 2012. Beige adipocytes are a distinct type of thermogenic fat cell in mouse and human. *Cell*, 150(2), pp.366–76. Available at: http://www.pubmedcentral.nih.gov/articlerender.fcgi?artid=3402601&tool=pmcentrez&rendertype=abstract [Accessed April 29, 2014].

You, Y. et al., 2008. Insulin, cGMP, and TGF-beta signals regulate food intake and quiescence in C. elegans: a model for satiety. *Cell metabolism*, 7(3), pp.249–57. Available at: http://www.pubmedcentral.nih.gov/articlerender.fcgi?artid=3786678&tool=pmcentrez&rendertype=abstract [Accessed April 28, 2014].

Zangwill, S.D. et al., 2006. Marfan syndrome type II: there is more to Marfan syndrome than fibrillin 1. *Congenit.Heart Dis.*, 1(1747-0803 (Electronic)), pp.229–232.